*The Canadian Mineralogist*
Vol. 43, pp. 1759-1780 (2005)

# THE SPINIFEX LAYER OF THE BOSTON CREEK FERROPICRITE, ABITIBI BELT, ONTARIO: MINERALOGICAL AND GEOCHEMICAL EVIDENCE FOR AN UNUSUAL HISTORY OF CLINOPYROXENE GROWTH AND MAGMA RECHARGE

JAMES H. CROCKET[§]

*School of Geography and Earth Sciences, McMaster University, Hamilton, Ontario L8S 4K1, Canada*

DAVID M. LENG

*Consulting geologist, Ancaster, Ontario L9G 1Z6, Canada*

DAVID J. GOOD

*Bootstrap Software Inc., Burlington, Ontario L7N 3M6, Canada*

WILLIAM E. STONE

*Geoinformatics Exploration Canada Ltd., Vancouver, British Columbia V6E 2T6, Canada*

MICHELLE S. STONE

*School of Earth and Geographical Sciences, University of Western Australia, Crawley, WA, Australia*

## ABSTRACT

The Boston Creek ferropicrite (BCF), exposed near Kirkland Lake in the Abitibi Belt, Ontario, is a differentiated layered mafic–ultramafic unit of Archean age with a remarkably thick layer of spinifex-textured clinopyroxenite at its stratigraphic top, comprising about one-third of a total thickness of ~100 m. The spinifex layer was sampled at intervals of ~1 m. Relict spinifex-textured igneous clinopyroxene occurs in the basal two-thirds of the layer. Results of electron-microprobe analyses show that the clinopyroxene is Ca-rich augite with rim domains usually higher in Fe, Ca and Mn than the core. These variations are most prominent in the basal 10 m of the layer. An overgrowth- and embayment-textured clinopyroxene has much larger core-to-rim variations, with compositions plotting as diopside and hedenbergite. The compositional variations in the spinifex-textured clinopyroxene are attributed to reaction between clinopyroxene and trapped interstitial melt. A metamorphic origin is considered much less likely owing to the lack of evidence for mass transfer between wallrocks and the BCF, the probability that exchange reactions between pyroxene and trapped melt (now groundmass) are favored by magmatic temperatures, and the high Mn content in pyroxene, found in the basal 5 m of the spinifex layer. Whole-rock compositions exhibit prominent depletion trends for Mg, Ni, Co and Cr in the top 3 m of the layer, and weak but distinct enrichment trends for Ca, Al, K and Ti, features reflecting the degree of compatibility of these elements during clinopyroxene/melt fractionation. In the basal 10 m, distinct compositional reversals are evident in whole-rock profiles of Mg, Al, Cr and Mg#. These reversals are thought to reflect a significant change in magma composition, possibly due to magma recharge during the gabbro stage, whereby injection and mixing of relatively unfractionated magma with residual melt occurred. Local variations in PGE abundances, aspects of Re–Os isotope systematics, and detailed magnetic characteristics of the basal spinifex and the upper gabbro layers support this proposal.

*Keywords*: Boston Creek ferropicrite, clinopyroxene spinifex, platinum-group elements, komatiite, magma recharge, Abitibi Belt, Ontario.

## SOMMAIRE

La ferropicrite de Boston Creek, affleurant près de Kirkland Lake dans la ceinture de l'Abitibi, en Ontario, est une unité différenciée à niveaux mafiques et ultramafiques d'âge archéen ayant une couche remarquablement épaisse de clinopyroxénite à texture spinifex à son contact supérieur, équivalant à environ un tiers de l'épaisseur totale d'environ 100 m. Nous avons échan-

§ *E-mail address*: crocketj@univmail.cis.mcmaster.ca

tillonné la section à spinifex à un intervalle d'environ 1 m. Des reliquats du clinopyroxène à spinifex sont présents dans les deux-tiers inférieurs de la couche. Les résultats des analyses avec une microsonde électronique montrent que le clinopyroxène est une augite calcique avec une bordure généralement enrichie en Fe, Ca et Mn par rapport au noyeau. Ces variations sont plus évidentes dans les 10 m à la base de la couche. Un second clinopyroxène en surcroissance et en invaginations montre des variations de coeur à la bordure encore plus marquées, avec des compositions atteingnant le domaine de la diopside et de l'hédenbergite. Les variations en composition du clinopyroxène à texture de spinifex sont attribuées à la réaction entre clinopyroxène et liquide interstitiel piégé. Une origine métamorphique semble beaucoup moins probable, compte tenu du manque de signes de tranferts de masse entre les roches encaissantes et la ferropicrite, la probabilité que les réactions d'échange entre pyroxène et liquide piégé (présentement la matrice) seraient favorisées par une température magmatique, et la teneur élevée en Mn dans les premiers 5 m à la base du niveau à texture spinifex. Les compositions globales témoignent de diminutions marquées en Mg, Ni, Co et Cr dans les premiers 3 m au haut de la couche, et de faibles enrichissements en Ca, Al, K et Ti, signes de l'incompatibilité de ces éléments au cours du fractionnement du clinopyroxène. Dans les premiers 10 m à la base de la couche, des inversions distinctes en composition sont évidentes dans les profils de Mg, Al, Cr et Mg# des roches totales. Ces inversions refléteraient un changement important de la composition du magma, peut-être à cause d'une venue de magma frais au stade de cristallisation du gabbro, et d'un mélange conséquent entre magma non fractionné et magma résiduel. Des variations locales des teneurs en éléments du groupe du platine, certains aspects des relations isotopiques entre Re et Os, et les caractéristiques magnétiques à la base de la zone à spinifex et de la partie supérieure de la couche gabbroïque viennent étayer cette hypothèse.

(Traduit par la Rédaction)

*Mots-clés*: ferropicrite de Boston Creek, spinifex à clinopyroxène, éléments du groupe du platine, komatiite, ré-injection de magma, ceinture de l'Abitibi, Ontario.

## Introduction

The Boston Creek ferropicritic basalt (BCF) is located near Kirkland Lake in the southern part of the Archean Abitibi greenstone belt (Fig. 1), and outcrops discontinuously over a strike length of almost 20 km with a maximum thickness of ~115 m. The BCF is a differentiated, layered body consisting of peridotite, clinopyroxenite, gabbro and spinifex-textured clinopyroxenite layers from stratigraphic base to top. Among its most interesting aspects is a spinifex-textured clinopyroxenite layer of up to 33 m thickness at the stratigraphic top of the unit. The BCF has been investigated in detail by Stone *et al*. (1987, 1992, 1993, 1995a, b, 1996, 2003, 2005), Larson (1994), Larson *et al*. (1998) and Walker & Stone (2001). These investigators concluded that: (1) the BCF parental magma is ferropicritic rather than komatiitic, (2) a very high Fe content at high Mg and low Al with high Ti, LREE and Nb at low HREE, Y and Sc is a geochemical signature of mantle origin rather than a result of contamination by crustal material, and (3) the BCF hosts three zones of Cu–Ag–Au–PGE mineralization containing platinum-group minerals with maximum PGE grades of ~0.8 g/t. A depleted Sm–Nd isotopic composition ($\varepsilon_{Nd}$ between 2 and 3; Stone *et al*. 1995b) and low initial Re–Os isotopic composition ($\gamma_{Os} = -4$; Walker & Stone 2001) indicate melting of a depleted mantle metasomatically enriched in Nb–LREE and Fe–Ti by hydrous fluids. The presence of positive Nb–Ta anomalies in primitive-mantle-normalized incompatible element profiles (Stone *et al*. 1995b) is inconsistent with a subduction-related origin for the BCF parental magma. Stone *et al*. (1995b) noted that most of these geochemical characteristics are similar to those of the ferropicritic basalts at Pechenga, Russia (Hanski 1992).

Stone *et al*. (1995a) provided details on the composition of three samples of spinifex-textured clinopyroxene. With the objective of mapping trends in mineral compositions and variations in whole-rock composition across the spinifex layer, in order to better understand the growth history of the layer of spinifex-textured clinopyroxene, a detailed sampling and analytical program across the layer on Transect 2 was carried out (Leng 1997). Petrographic studies, electron-microprobe analyses of core and rim domains in clinopyroxene, and whole-rock chemical analyses were completed on samples taken at ~1 m intervals across the entire spinifex layer. Relict igneous clinopyroxene occurs from 13 to 30 m below the top of the spinifex. Core-to-rim profiles across the clinopyroxene grains are taken to reflect reaction between primary magmatic clinopyroxene and an increasingly fractionated residual gabbroic melt, possibly modified by fresh injection of magma during growth of the basal 10 m of the spinifex layer. Two samples included a compositionally and texturally distinct variety of clinopyroxene occurring as embayments into and overgrowths on spinifex-textured clinopyroxene. Such pyroxene is a product of alteration of the spinifex-textured clinopyroxene, possibly produced by aqueous fluids at ~500°C.

## Analytical Procedures

### *Analysis of the minerals*

Clinopyroxene compositions were determined on a JEOL JXA–8600 electron microprobe at the University of Western Ontario (Tables 1, 2). Analyses were performed in wavelength-dispersion mode at an accelerating voltage of 15 kV, a current of 10.5 nA, and a beam diameter of 1 μm. Count times of 20 seconds were

utilized for Ca, Fe, Mg, Ti, Na and Cr, and 30 seconds for Si, Al, and Mn. Matrix corrections were performed on line with the Noran ZAF program. Natural silicate and oxide minerals were utilized as standards. Quality control was maintained by replicate analyses of mineral standards that indicated precision and accuracy relative to absolute oxide concentration of at least 0.5 wt.%.

*Whole-rock analyses*

Whole-rock analyses for major, minor, and trace elements were undertaken by Activation Laboratories Ltd, Ancaster, Ontario. A variety of techniques were employed, mainly lithium metaborate–tetraborate fusion and total acid (HCl, $HNO_3$, $HClO_4$ and HF)

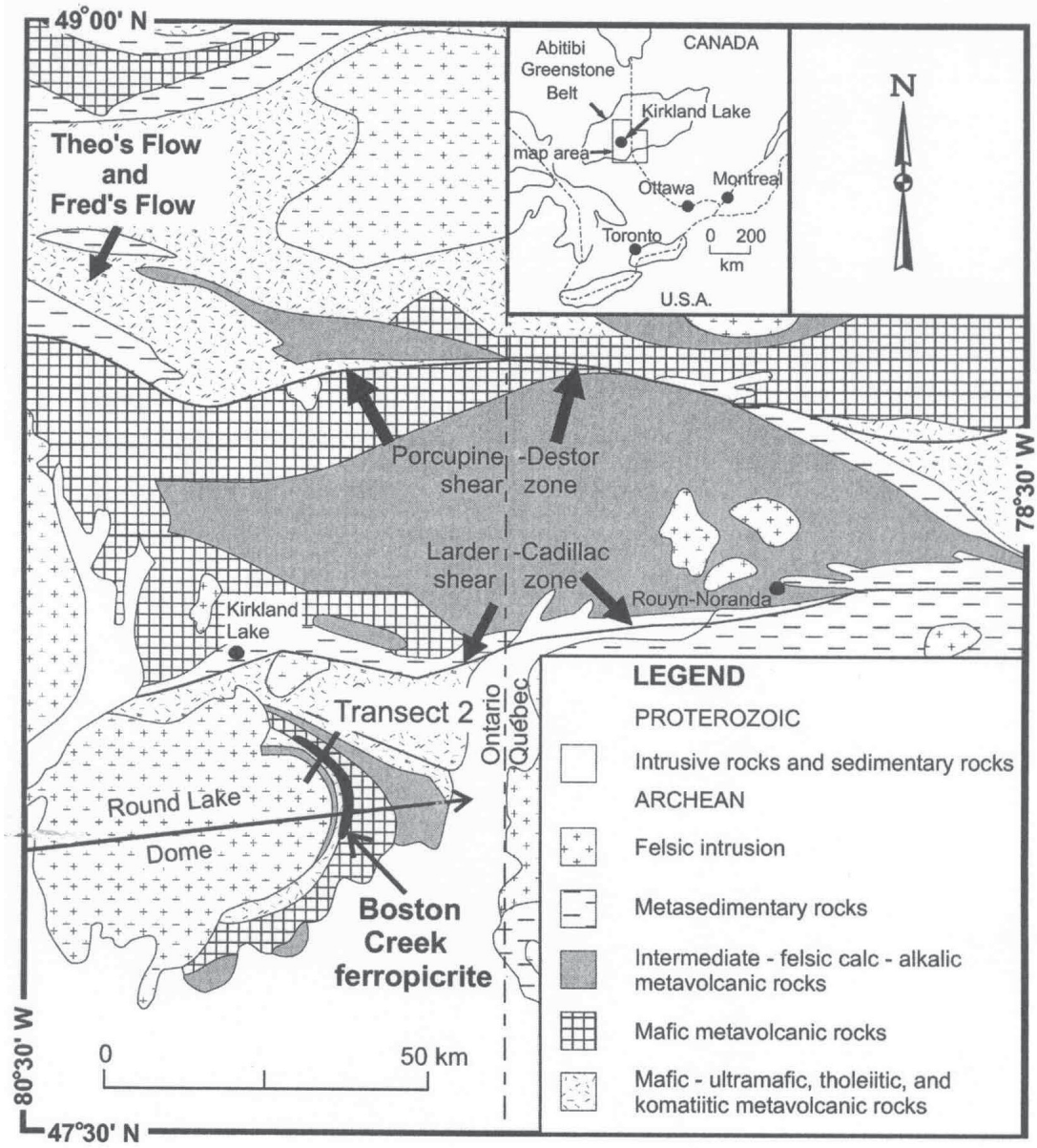


FIG. 1. Location map for the Boston Creek ferropicrite showing position of Transect 2 in the northwestern part of the unit (after Stone *et al*. 1996). The locations of Fred's Flow komatiitic basalt and Theo's Flow tholeiitic basalt, Munro Township, also are shown.

TABLE 1. AVERAGE COMPOSITIONS OF CORE AND RIM OF SPINIFEX CLINOPYROXENE, BOSTON CREEK FERROPICRITE

| Sample | 12 | | 14 | | 17 | | 18 | | 19 | | 20 | | 21 | | 22 | | 23 | | 24 | |
|---|---|---|---|---|---|---|---|---|---|---|---|---|---|---|---|---|---|---|---|---|
| Depth (m) | 13.1 | | 16.5 | | 21.0 | | 22.0 | | 23.5 | | 25.3 | | 26.5 | | 27.7 | | 28.7 | | 29.9 | |
| Grains | 2 | 2 | 3 | 2 | 2 | 2 | 4 | 4 | 6 | 6 | 5 | 4 | 7 | 6 | 4 | 4 | 8 | 6 | 4 | 4 |
| Domain | C | R | C | R | C | R | C | R | C | R | C | R | C | R | C | R | C | R | C | R |
| *n* | 2 | 4 | 4 | 4 | 2 | 4 | 9 | 9 | 8 | 12 | 11 | 8 | 11 | 10 | 20 | 7 | 10 | 11 | 9 | 10 |
| $SiO_2$ wt% | 51.54 | 51.28 | 52.30 | 52.17 | 52.97 | 52.34 | 51.92 | 51.63 | 52.18 | 52.16 | 51.48 | 51.59 | 51.34 | 51.34 | 52.19 | 51.20 | 52.64 | 52.42 | 52.26 | 52.03 |
| $TiO_2$ | 0.70 | 0.65 | 0.48 | 0.46 | 0.40 | 0.45 | 0.58 | 0.61 | 0.50 | 0.53 | 0.65 | 0.55 | 0.62 | 0.63 | 0.45 | 0.67 | 0.47 | 0.48 | 0.44 | 0.41 |
| $Al_2O_3$ | 2.59 | 2.69 | 1.79 | 1.78 | 1.57 | 1.59 | 2.22 | 2.23 | 1.83 | 1.92 | 2.26 | 1.91 | 2.47 | 2.38 | 1.66 | 2.27 | 1.57 | 1.63 | 1.54 | 1.67 |
| $Cr_2O_3$ | 0.21 | 0.27 | 0.16 | 0.18 | 0.28 | 0.34 | 0.23 | 0.18 | 0.25 | 0.12 | 0.15 | 0.09 | 0.07 | 0.06 | 0.14 | 0.08 | 0.19 | 0.15 | 0.08 | 0.07 |
| FeO | 7.46 | 8.07 | 7.21 | 7.50 | 7.84 | 7.07 | 7.85 | 8.57 | 7.13 | 7.85 | 8.01 | 9.22 | 8.91 | 9.74 | 7.79 | 9.29 | 7.10 | 7.51 | 9.12 | 9.23 |
| MnO | 0.15 | 0.15 | 0.16 | 0.16 | 0.14 | 0.15 | 0.15 | 0.14 | 0.23 | 0.21 | 0.13 | 0.25 | 0.17 | 0.31 | 0.20 | 0.27 | 0.15 | 0.15 | 0.33 | 0.26 |
| MgO | 14.52 | 14.51 | 15.08 | 15.03 | 15.24 | 15.24 | 14.80 | 14.15 | 15.05 | 14.67 | 14.31 | 13.46 | 13.89 | 13.35 | 14.52 | 13.22 | 13.84 | 14.64 | 13.41 | 13.32 |
| CaO | 22.51 | 22.22 | 22.47 | 22.51 | 22.71 | 22.57 | 22.54 | 22.43 | 22.38 | 22.51 | 22.44 | 22.61 | 22.19 | 22.40 | 22.78 | 22.66 | 22.95 | 22.81 | 22.93 | 22.74 |
| $Na_2O$ | 0.40 | 0.42 | 0.39 | 0.37 | 0.35 | 0.37 | 0.42 | 0.44 | 0.38 | 0.40 | 0.36 | 0.37 | 0.42 | 0.48 | 0.38 | 0.34 | 0.17 | 0.27 | 0.31 | 0.37 |
| Total | 100.08 | 100.26 | 100.04 | 100.16 | 101.50 | 100.11 | 100.71 | 100.38 | 99.92 | 100.37 | 99.79 | 100.05 | 100.08 | 100.68 | 100.11 | 100.00 | 99.07 | 100.05 | 100.41 | 100.10 |
| Mg# | 77.3 | 76.5 | 78.5 | 77.8 | 77.3 | 79.0 | 76.5 | 74.3 | 78.5 | 76.4 | 75.8 | 71.4 | 72.9 | 70.1 | 77.8 | 71.1 | 78.6 | 77.2 | 77.2 | 70.8 |
| En mol.% | 43.5 | 43.7 | 44.3 | 44.1 | 44.1 | 44.8 | 43.8 | 42.1 | 44.5 | 43.2 | 42.6 | 40.0 | 41.6 | 40.1 | 42.7 | 39.7 | 40.7 | 42.7 | 39.4 | 39.4 |
| Fs | 12.5 | 13.6 | 11.9 | 12.4 | 12.7 | 11.7 | 13.0 | 14.3 | 11.8 | 13.0 | 13.4 | 15.4 | 15.0 | 16.4 | 12.8 | 15.6 | 11.7 | 12.3 | 15.0 | 15.3 |
| Wo | 43.9 | 42.7 | 43.9 | 43.5 | 43.2 | 43.6 | 43.1 | 43.5 | 43.7 | 43.9 | 44.0 | 44.6 | 43.5 | 43.5 | 44.5 | 44.7 | 47.6 | 45.0 | 45.5 | 45.3 |

C: core domains, R: rim domains, *n*: number of electron-microprobe analyses made. Symbols: En: enstatite, Fs: ferrosilite, Wo: wollastonite.

TABLE 2. COMPOSITIONS OF EMBAYMENT AND OVERGROWTH CLINOPYROXENE, SPINIFEX LAYER, BOSTON CREEK FERROPICRITE

| Sample | 20 | | 22 | |
|---|---|---|---|---|
| Depth (m) | 25.3 | | 27.7 | |
| Type | O | E | E | s.d. |
| Grains (ave. of *n*) | 2 | 1 | 8 | |
| $SiO_2$ wt% | 52.40 | 48.14 | 50.71 | 0.93 |
| $TiO_2$ | 0.055 | 0.85 | 0.18 | 0.11 |
| $Al_2O_3$ | 0.73 | 3.68 | 1.72 | 1.20 |
| $Cr_2O_3$ | 0.07 | 0.03 | 0.05 | 0.03 |
| FeO | 12.02 | 17.06 | 16.74 | 2.22 |
| MnO | 0.57 | 0.39 | 0.54 | 0.39 |
| MgO | 10.97 | 7.62 | 7.80 | 1.25 |
| CaO | 22.73 | 21.31 | 21.99 | 0.50 |
| $Na_2O$ | 0.66 | 0.51 | 0.85 | 0.26 |
| Total | 100.20 | 100.20 | 100.6 | |
| Mg# | 61.9 | 44.3 | 45.4 | |
| En mol.% | 33.5 | 27.4 | 24.9 | |
| Fs | 18.7 | 31.3 | 27.0 | |
| Wo | 47.8 | 41.3 | 48.1 | |

O: overgrowth, E: embayment; *n*: number of analyses made. s.d.: standard deviation. Symbols: En: enstatite, Fs: ferrosilite, Wo: wollastonite.

dissolution (TAD), with analysis by inductively coupled plasma – mass spectrometry (ICP–MS). Other methods included NiS and Pb fire assays with instrumental neutron activation analysis (INAA) and ICP–MS, respectively, for determination of the concentration of the PGE and Au. All samples were analyzed together with international reference standards (rocks MAG1, BIR1, W2, MGR1, GXR1, UTM1, SARM7) for calibration. Levels of some trace elements were determined by more than one procedure, in which case values in Table 3 are the average of different methods.

All data are reported as anhydrous values calculated by subtracting the loss on ignition (LOI) from the analytical total and normalizing this result to 100%. The iron oxide values are calculated as FeO = 90% of total iron (*e.g.*, Hanski 1992). Major elements were determined by Li borate fusion at detection limits of 0.01 wt.%, except for Ti, where the limit was 0.001 wt.%. The LOI is a gravimetric analysis after 24 hours heating at 850°C. Values of $Cr_2O_3$ are the average of Li borate fusion and INAA, with detection limits of 0.002 and 0.0001 wt.%, respectively.

With the exception of the PGE, Au, Ag, As, Se and S, 33 other minor and trace elements were determined by Li borate fusion. Levels of several of these elements were established by other methods in addition to Li borate fusion. These include Cu (TAD), Co (INAA), Ni (INAA, TAD), V (TAD) and Zn (INAA, TAD), where the additional methods are shown in parentheses. Values for these elements (Table 3) are the average of all methods employed. A qualitative assessment of how well the samples were analyzed for these elements at the concentrations in the BCF suite is made by comparing

the detection limit for a given element with the values obtained. Using the lowest value obtained for each element and the detection limit quoted by Activation Laboratories Ltd, the ratio (lowest value/detection limit) is calculated. For Rb, this ratio is (1.2 / 0.01) = 120, and indicates that for all 23 samples, Rb concentration

TABLE 3. WHOLE-ROCK CHEMICAL COMPOSITIONS OF THE SPINIFEX-TEXTURED LAYER OF THE BOSTON CREEK FERROPICRITE

| Sample | 1 | 2 | 4 | 5 | 6 | 7 | 8 | 9 | 10 | 11 | 12 | 13 |
|---|---|---|---|---|---|---|---|---|---|---|---|---|
| Depth (m) | 0 | 0.91 | 1.8 | 2.4 | 4.2 | 5.5 | 6.7 | 8.8 | 10.4 | 11.6 | 13.1 | 14.6 |
| $SiO_2$ wt% | 43.00 | 48.12 | 48.29 | 47.64 | 48.23 | 47.93 | 49.26 | 47.66 | 49.18 | 47.93 | 49.22 | 49.29 |
| $TiO_2$ | 1.11 | 1.08 | 1.29 | 1.52 | 1.35 | 1.37 | 1.44 | 1.39 | 1.36 | 1.46 | 1.45 | 1.32 |
| $Al_2O_3$ | 6.29 | 6.04 | 7.52 | 7.79 | 7.99 | 7.76 | 9.24 | 8.25 | 8.01 | 8.05 | 8.57 | 8.71 |
| $Fe_2O_3$ | 2.35 | 1.93 | 1.89 | 1.96 | 2.03 | 2.00 | 1.89 | 1.76 | 2.02 | 1.70 | 2.04 | 1.97 |
| FeO | 19.16 | 15.76 | 16.01 | 16.58 | 16.32 | 15.37 | 14.37 | 16.45 | 13.88 | 16.65 | 16.02 | 14.81 |
| MnO | 0.31 | 0.27 | 0.29 | 0.28 | 0.30 | 0.30 | 0.28 | 0.27 | 0.28 | 0.28 | 0.25 | 0.27 |
| MgO | 11.08 | 15.24 | 11.29 | 11.88 | 9.33 | 8.65 | 8.33 | 9.69 | 8.47 | 9.51 | 8.58 | 9.04 |
| CaO | 16.60 | 11.44 | 12.20 | 11.41 | 12.95 | 15.01 | 12.85 | 12.68 | 14.75 | 12.55 | 11.48 | 12.29 |
| $Na_2O$ | 0.61 | 0.47 | 1.53 | 1.22 | 1.80 | 1.97 | 2.71 | 1.82 | 2.56 | 1.82 | 2.65 | 2.60 |
| $K_2O$ | 0.09 | 0.11 | 0.12 | 0.15 | 0.23 | 0.22 | 0.21 | 0.23 | 0.19 | 0.23 | 0.29 | 0.27 |
| $P_2O_5$ | 0.09 | 0.11 | 0.08 | 0.10 | 0.09 | 0.08 | 0.06 | 0.13 | 0.12 | 0.09 | 0.10 | 0.12 |
| $Cr_2O_3$ | 0.172 | 0.117 | 0.129 | 0.073 | 0.062 | 0.072 | 0.065 | 0.048 | 0.066 | 0.067 | 0.065 | 0.055 |
| LOI | 6.11 | 3.64 | 3.75 | 2.33 | 2.56 | 1.58 | 3.07 | 2.61 | 1.35 | 3.66 | 1.38 | 1.30 |
| AT | 98.55 | 99.86 | 98.70 | 100.8 | 101.0 | 100.6 | 97.84 | 100.9 | 99.30 | 100.7 | 100.6 | 100.2 |
| Mg# | 50.76 | 63.29 | 55.70 | 56.08 | 50.46 | 50.07 | 50.84 | 51.22 | 52.12 | 50.47 | 48.85 | 52.10 |
| Rb (ppm) | 1.2 | 3.9 | 2.1 | 2.3 | 2.1 | 2.5 | 1.5 | 2 | 1.3 | 5.0 | 7.6 | 3.7 |
| Cs | 0.2 | 0.6 | 0.2 | 0.6 | 0.1 | <0.1 | <0.1 | 0.1 | 0.2 | 0.3 | 0.6 | 0.2 |
| Sr | 141 | 59 | 93 | 53 | 189 | 232 | 177 | 141 | 177 | 139 | 150 | 163 |
| Ba | 25.5 | 16 | 25.5 | 21 | 34 | 38 | 46.5 | 51 | 53.5 | 59 | 73 | 63 |
| La | 12.8 | 6.47 | 13.9 | 12.0 | 15.5 | 13.3 | 14.0 | 14.8 | 13.9 | 13.30 | 14.4 | 16.5 |
| Ce | 26.8 | 16.2 | 30.1 | 25.9 | 33.6 | 29 | 30.8 | 32.5 | 30.2 | 29.3 | 30.8 | 34.7 |
| Pr | 3.255 | 2.345 | 3.634 | 3.372 | 4.154 | 3.624 | 3.857 | 4.106 | 3.79 | 3.752 | 4.064 | 4.472 |
| Nd | 14.2 | 11.5 | 16.0 | 15.2 | 18.9 | 16.4 | 17.8 | 18.3 | 17.2 | 17.6 | 18.6 | 19.9 |
| Sm | 3.22 | 2.90 | 3.71 | 3.50 | 4.16 | 3.72 | 4.12 | 4.22 | 3.96 | 4.17 | 4.39 | 4.47 |
| Eu | 1.12 | 1.129 | 1.111 | 0.968 | 1.225 | 1.138 | 1.249 | 1.214 | 1.227 | 1.206 | 1.322 | 1.265 |
| Gd | 2.98 | 2.81 | 3.60 | 3.43 | 3.86 | 3.53 | 3.90 | 3.89 | 3.58 | 3.96 | 4.44 | 4.37 |
| Tb | 0.47 | 0.45 | 0.57 | 0.56 | 0.63 | 0.57 | 0.64 | 0.66 | 0.59 | 0.65 | 0.68 | 0.66 |
| Dy | 2.57 | 2.53 | 3.14 | 3.16 | 3.45 | 3.12 | 3.55 | 3.56 | 3.24 | 3.60 | 3.74 | 3.68 |
| Ho | 0.48 | 0.48 | 0.60 | 0.61 | 0.66 | 0.59 | 0.67 | 0.67 | 0.62 | 0.68 | 0.70 | 0.68 |
| Er | 1.27 | 1.32 | 1.63 | 1.68 | 1.80 | 1.63 | 1.84 | 1.85 | 1.71 | 1.92 | 1.92 | 1.86 |
| Tm | 0.184 | 0.189 | 0.243 | 0.249 | 0.261 | 0.238 | 0.262 | 0.267 | 0.255 | 0.286 | 0.288 | 0.278 |
| Yb | 1.13 | 1.16 | 1.50 | 1.54 | 1.65 | 1.51 | 1.73 | 1.69 | 1.57 | 1.74 | 1.80 | 1.71 |
| Lu | 0.164 | 0.174 | 0.224 | 0.230 | 0.246 | 0.225 | 0.253 | 0.251 | 0.230 | 0.260 | 0.264 | 0.256 |
| Y | 15 | 15 | 18.5 | 19 | 19.5 | 18 | 21.5 | 20.5 | 19 | 22 | 23 | 25.5 |
| Nb | 9.3 | 7.6 | 10 | 11 | 12 | 11 | 9.8 | 12 | 10 | 12 | 15 | 13 |
| Ta | 0.66 | 0.55 | 0.78 | 0.80 | 0.87 | 0.76 | 0.81 | 0.85 | 0.75 | 0.90 | 0.97 | 0.92 |
| Zr | 52 | 49.5 | 61 | 66.5 | 67 | 62.5 | 64 | 67 | 61 | 70.5 | 76 | 74 |
| Hf | 1.5 | 1.4 | 1.8 | 1.9 | 2.0 | 1.9 | 1.9 | 2.0 | 1.9 | 2.1 | 2.3 | 2.0 |
| Th | 1.14 | 0.92 | 1.21 | 1.17 | 1.34 | 1.21 | 1.25 | 1.24 | 1.19 | 1.31 | 1.33 | 1.32 |
| U | 0.23 | 0.21 | 0.27 | 0.27 | 0.32 | 0.27 | 0.28 | 0.29 | 0.26 | 0.31 | 0.31 | 0.31 |
| V | 184 | 202 | 219 | 247 | 235 | 240 | 231 | 258 | 239 | 261 | 248 | 245 |
| Cr | 1065 | 761 | 474 | 409 | 485 | 428 | 308 | 442 | 435 | 432 | 366 | 416 |
| Sc | 30 | 38.5 | 33.5 | 34 | 35 | 37 | 33 | 38.5 | 39 | 40 | 36 | 39 |
| Ni | 886 | 615 | 263 | 273 | 316 | 252 | 161 | 258 | 196 | 189 | 210 | 184 |
| Co | 129 | 115 | 60 | 80 | 88 | 79 | 62 | 82 | 73 | 73 | 76 | 64 |
| Cu | 563 | 314 | 135 | 271 | 316 | 345 | 324 | 305 | 324 | 247 | 245 | 255 |
| Zn | 206 | 203 | 124 | 227 | 192 | 170 | 138 | 127 | 130 | 148 | 157 | 106 |
| Ag | 0.5 | 0.7 | <0.4 | <0.4 | 1 | <0.4 | <0.4 | 0.6 | 0.4 | <0.4 | <0.4 | 0.7 |
| As | 14 | 4.5 | 2.5 | 0.49 | 2.8 | 2.0 | 1.0 | 0.49 | 0.49 | 1.0 | 1.3 | 0.49 |
| Sb | 0.57 | 0.37 | 0.17 | 0.47 | 0.27 | 0.31 | 0.59 | 0.16 | 0.18 | 0.29 | 0.61 | 0.59 |
| Sn | 0.8 | 0.7 | <0.5 | 1.1 | 0.7 | 0.7 | <0.5 | 0.9 | 0.7 | 0.7 | 1.0 | 0.6 |
| Se | 1.2 | 0.3 | <0.1 | 0.2 | 0.4 | 0.1 | 0.4 | 0.3 | 0.4 | 0.3 | 0.3 | 0.4 |
| S | 1.17% | 2200 | 2700 | 1500 | 4000 | 3000 | 2600 | 700 | 700 | 800 | 1100 | 1100 |
| Ir (ppb) | 0.6 | 0.2 | 0.2 | n.d. | 0.1 | n.d. | 0.1 | n.d. | 0.1 | n.d. | 0.1 | n.d. |
| Ru | 2.6 | 0.1 | 1.60 | n.d. | 0.1 | n.d. | <0.1 | n.d. | <0.2 | n.d. | <0.2 | n.d. |
| Rh | 0.9 | 0.4 | 0.8 | n.d. | 0.6 | n.d. | 0.5 | n.d. | 0.5 | n.d. | 0.5 | n.d. |
| Pt | 7.5 | 4.1 | 5.7 | 6.9 | 5.9 | 7.0 | 5.5 | 6.6 | 5.0 | 7.5 | 5.0 | 6.1 |
| Pd | 8.7 | 4.4 | 6.3 | 4.8 | 6.0 | 6.1 | 5.9 | 5.4 | 5.1 | 6.8 | 4.3 | 4.2 |
| Au[1] | 163, 12 | <0.1 | 0.7 | n.d. | 0.7 | n.d. | 0.2 | n.d. | <0.3 | n.d. | 1.0 | n.d. |

TABLE 3 (cont'd). WHOLE-ROCK CHEMICAL COMPOSITIONS OF THE SPINIFEX-TEXTURED LAYER OF THE BOSTON CREEK FERROPICRITE

| Sample | 14 | 15 | 16 | 17 | 18 | 19 | 20 | 21 | 22 | 23 | 24 | Average |
|---|---|---|---|---|---|---|---|---|---|---|---|---|
| Depth (m) | 16.5 | 17.9 | 19.8 | 21 | 22 | 23.5 | 25.3 | 26.5 | 27.7 | 28.7 | 29.9 | |
| $SiO_2$ wt% | 48.49 | 49.70 | 47.11 | 48.03 | 49.25 | 48.62 | 50.66 | 48.99 | 49.63 | 48.58 | 50.80 | 48.51 |
| $TiO_2$ | 1.35 | 1.34 | 1.56 | 1.42 | 1.33 | 1.56 | 1.20 | 1.32 | 1.26 | 1.56 | 0.92 | 1.35 |
| $Al_2O_3$ | 8.19 | 8.74 | 7.74 | 8.82 | 8.64 | 9.54 | 9.82 | 8.94 | 8.11 | 6.79 | 5.78 | 8.06 |
| $Fe_2O_3$ | 1.82 | 1.95 | 1.83 | 2.07 | 1.92 | 1.87 | 2.03 | 1.82 | 1.88 | 1.77 | 1.82 | 1.93 |
| MnO | 0.27 | 0.25 | 0.26 | 0.25 | 0.27 | 0.29 | 0.21 | 0.25 | 0.28 | 0.27 | 0.24 | 0.27 |
| MgO | 9.57 | 8.67 | 10.88 | 9.89 | 8.36 | 7.77 | 6.56 | 7.55 | 8.86 | 9.67 | 10.87 | 9.55 |
| CaO | 12.46 | 11.73 | 12.21 | 12.13 | 12.81 | 10.98 | 11.00 | 12.99 | 13.23 | 15.07 | 16.05 | 12.91 |
| $Na_2O$ | 2.04 | 3.04 | 1.49 | 2.13 | 2.45 | 2.84 | 4.07 | 3.06 | 2.55 | 1.68 | 1.68 | 2.12 |
| $K_2O$ | 0.27 | 0.27 | 0.28 | 0.28 | 0.25 | 0.28 | 0.28 | 0.20 | 0.25 | 0.18 | 0.11 | 0.22 |
| $P_2O_5$ | 0.09 | 0.11 | 0.09 | 0.10 | 0.07 | 0.12 | 0.10 | 0.11 | 0.12 | 0.09 | 0.07 | 0.10 |
| $Cr_2O_3$ | 0.063 | 0.066 | 0.065 | 0.064 | 0.068 | 0.044 | 0.038 | 0.027 | 0.030 | 0.057 | 0.048 | 0.070 |
| LOI | 1.60 | 1.50 | 2.31 | 1.86 | 1.82 | 1.39 | 0.91 | 0.96 | 1.34 | 0.57 | 0.85 | 2.11 |
| AT | 100.6 | 98.59 | 100.8 | 101.0 | 99.75 | 100.6 | 100.9 | 100.5 | 100.7 | 99.39 | 100.6 | |
| Mg# | 51.79 | 50.97 | 53.40 | 53.03 | 49.43 | 45.51 | 44.13 | 46.83 | 52.23 | 53.74 | 60.96 | 51.91 |
| Rb (ppm) | 3.3 | 2.7 | 2.2 | 6.6 | 1.9 | 4.1 | 3.5 | 2.0 | 4.8 | 1.5 | 2.5 | 3.0 |
| Cs | 0.2 | 0.2 | 0.3 | 0.4 | 0.1 | 0.2 | <0.1 | 0.1 | 0.2 | <0.1 | 0.1 | 0.26 |
| Sr | 146 | 159 | 133 | 132 | 165 | 227 | 411 | 242 | 259 | 189 | 138 | 170 |
| Ba | 65.5 | 64.5 | 69 | 78 | 67.5 | 89 | 130 | 55 | 104 | 42 | 56.5 | 57.7 |
| La | 14.8 | 14.8 | 13.7 | 13.2 | 14.5 | 16.8 | 16.5 | 16.1 | 12.9 | 13.6 | 9.28 | 13.8 |
| Ce | 31.4 | 32 | 29.7 | 28.6 | 30.7 | 35.7 | 35.6 | 33.7 | 27.6 | 29.8 | 20.1 | 29.8 |
| Pr | 4.017 | 4.127 | 3.987 | 3.752 | 3.947 | 4.558 | 4.51 | 4.301 | 3.573 | 3.885 | 2.63 | 3.81 |
| Nd | 18.0 | 18.6 | 18.5 | 17.1 | 17.3 | 19.9 | 19.7 | 19.0 | 16.7 | 17.3 | 12.4 | 17.2 |
| Sm | 4.09 | 4.19 | 4.43 | 4.04 | 3.99 | 4.62 | 4.50 | 4.37 | 3.89 | 3.96 | 3.04 | 3.99 |
| Eu | 1.166 | 1.245 | 1.293 | 1.138 | 1.194 | 1.356 | 1.254 | 1.317 | 1.118 | 1.016 | 0.879 | 1.18 |
| Gd | 3.92 | 4.18 | 4.31 | 3.81 | 3.77 | 4.41 | 4.17 | 4.13 | 3.83 | 3.79 | 2.88 | 3.81 |
| Tb | 0.61 | 0.65 | 0.68 | 0.64 | 0.6 | 0.71 | 0.67 | 0.64 | 0.62 | 0.6 | 0.47 | 0.61 |
| Dy | 3.39 | 3.53 | 3.77 | 3.52 | 3.33 | 3.98 | 3.69 | 3.55 | 3.35 | 3.35 | 2.63 | 3.37 |
| Ho | 0.63 | 0.68 | 0.70 | 0.68 | 0.63 | 0.76 | 0.69 | 0.67 | 0.64 | 0.62 | 0.50 | 0.64 |
| Er | 1.78 | 1.89 | 1.95 | 1.86 | 1.77 | 2.08 | 1.94 | 1.83 | 1.75 | 1.72 | 1.38 | 1.76 |
| Tm | 0.261 | 0.279 | 0.294 | 0.277 | 0.257 | 0.302 | 0.275 | 0.261 | 0.253 | 0.255 | 0.201 | 0.26 |
| Yb | 1.60 | 1.72 | 1.78 | 1.72 | 1.55 | 1.88 | 1.75 | 1.68 | 1.65 | 1.57 | 1.24 | 1.60 |
| Lu | 0.236 | 0.256 | 0.260 | 0.251 | 0.235 | 0.285 | 0.270 | 0.252 | 0.241 | 0.236 | 0.180 | 0.24 |
| Y | 20.5 | 21 | 22.5 | 21 | 21 | 24.5 | 21.5 | 21.5 | 20.5 | 19.5 | 15 | 20.2 |
| Nb | 12 | 12 | 12 | 12 | 12 | 14 | 13 | 12 | 12 | 8.7 | 7.3 | 11.3 |
| Ta | 0.81 | 0.87 | 0.90 | 0.87 | 0.81 | 1.02 | 0.95 | 0.84 | 0.85 | 0.67 | 0.51 | 0.81 |
| Zr | 67.5 | 68.5 | 73 | 71.5 | 64.5 | 83 | 76 | 70 | 66.5 | 59.5 | 47 | 66.0 |
| Hf | 1.9 | 2.0 | 2.1 | 2.0 | 1.9 | 2.4 | 2.1 | 2.0 | 1.9 | 1.8 | 1.5 | 1.93 |
| Th | 1.17 | 1.29 | 1.28 | 1.19 | 1.12 | 1.54 | 1.39 | 1.23 | 1.00 | 1.11 | 0.79 | 1.21 |
| U | 0.28 | 0.31 | 0.30 | 0.29 | 0.27 | 0.35 | 0.28 | 0.30 | 0.25 | 0.24 | 0.18 | 0.28 |
| V | 254 | 221 | 288 | 255 | 240 | 264 | 210 | 244 | 239 | 337 | 229 | 243 |
| Cr | 441 | 424 | 424 | 454 | 290 | 252 | 185 | 200 | 387 | 318 | 291 | 421 |
| Sc | 39.5 | 36 | 45 | 41 | 34 | 32 | 31 | 36.5 | 43.5 | 45.5 | 57.5 | 38 |
| Ni | 217 | 157 | 209 | 212 | 151 | 145 | 151 | 152 | 204 | 184 | 254 | 254 |
| Co | 80 | 61 | 87 | 78 | 64 | 64 | 66 | 73 | 62 | 79 | 72 | 77 |
| Cu | 304 | 276 | 457 | 298 | 338 | 307 | 257 | 316 | 153 | 388 | 179 | 301 |
| Zn | 137 | 95 | 162 | 126 | 125 | 100 | 120 | 84 | 127 | 120 | 133 | 142 |
| Ag | <0.4 | <0.4 | 0.5 | 0.6 | 0.6 | <0.4 | 0.5 | 0.5 | 0.6 | 0.7 | 0.4 | n.d. |
| As | 1.4 | 0.49 | 0.9 | 0.8 | 0.49 | 1.1 | 1.2 | 0.49 | 0.49 | 0.49 | 0.49 | 1.71 |
| Sb | 0.14 | 0.25 | 0.17 | 0.23 | 0.22 | 0.17 | 0.14 | 0.23 | 0.34 | 0.22 | 0.34 | 0.31 |
| Sn | 1.0 | 0.5 | 0.8 | 0.8 | 0.6 | 0.6 | 3.2 | 1.0 | 0.7 | 0.5 | 0.7 | 0.87 |
| Se | 0.4 | 0.5 | 0.5 | 0.2 | 0.6 | 0.5 | 0.4 | 0.2 | 0.4 | 0.3 | 0.3 | 0.39 |
| S | 1100 | 1500 | 1800 | 1000 | 1000 | 1300 | 700 | 700 | 500 | 800 | 400 | n.d. |
| Ir (ppb) | 0.1 | n.d. | 0.2 | n.d. | 0.15 | n.d. | 0.1 | n.d. | 0.1 | n.d. | 0.2 | n.d. |
| Ru | 0.1 | n.d. | 0.6 | n.d. | 0.2 | n.d. | <0.1 | n.d. | 0.3 | n.d. | 6.1 | n.d. |
| Rh | 0.6 | n.d. | 0.9 | n.d. | 0.6 | n.d. | 0.6 | n.d. | 0.7 | n.d. | 0.4 | n.d. |
| Pt | 5.5 | 6.2 | 7.3 | 6.1 | 6.4 | 7.4 | 5.5 | 6.9 | 4.7 | 5.9 | 3.6 | 6.0 |
| Pd | 6.8 | 3.6 | 7.2 | 4.6 | 5.9 | 5.8 | 6.1 | 4.9 | 4.5 | 2.1 | 2.2 | 5.3 |
| Au | 0.8 | n.d. | 1.1 | n.d. | 1.3 | n.d. | <0.1 | n.d. | 0.1 | n.d. | 1.7 | n.d. |

The compositions are normalized on an anhydrous basis. Mg#: molar 100 (MgO/[MgO + FeO]); the ratio $FeO:Fe_2O_3$ is taken to be 9:1 (Hanski 1992). AT: analytical total.
<0.1: not detected at the concentration limit indicated; n.d.: not determined.
[1] average of 163 ppb and 12 ppb, determined on two separate 16 g aliquots of the sample.

is at least 120 times the detection limit. For minor elements with all values above the detection limit (31 of 33 samples), the average of all such ratios is 150, with a range of 3 to 600. Two elements, Cs and Sn, each of which include several samples at the detection limit are excluded. Thus, for the levels of trace elements established by Li borate fusion, the methodology is of adequate sensitivity, except for the Cs and Sn determinations for some samples.

For the PGE and Au, two fire-assay procedures including NiS with detection limits of 0.1 ppb for all elements and Pb fire assay for Pd and Pt with the same detection limits were employed. Average Pt and Pd values for the two assays (Table 3) are ~20 to 80 times the detection limit. Values for Rh are four to nine times the detection limit. Detection limits for Ir and Ru are less satisfactory, with 50 and 60% of samples at least twice the detection limits.

In regards to the remaining elements, Ag (TAD) and As (INAA) are poorly determined, with 50% of samples above the detection limits. Selenium ($HNO_3 - H_2O_2$ digestion) and S (Infrared) are well determined, with all samples at least four times the detection limit for S and only two samples at the detection limit for Se.

## Petrography of the Spinifex-Textured Layer

Despite the conversion to amphibolite, primary igneous textures and in the basal 10 to 12 m of the primary clinopyroxene layer are well preserved. The spinifex textures are defined exclusively by clinopyroxene. Although ultramafic and moderately magnesian, the rocks lack evidence of modal olivine or pseudomorphs thereof. The spinifex-textured layer consists of three texturally distinct zones (Fig. 2): (1) chilled margin zone, (2) random spinifex zone, and (3) oriented spinifex zone.

### *Chilled margin zone*

The chilled margin is the uppermost zone (Fig. 2). At 50 cm thick, it is also the thinnest. The rock (sample #1) is highly altered and weakly deformed, but appears to have consisted of hollow, randomly oriented, isolated grains and fan-like sheaves (3–6 grains) of fine-grained clinopyroxene (10–20 modal %), minor chromite, and pyrite in a "glassy" groundmass. The clinopyroxene is replaced by green amphibole of low Ti, Al and alkali content relative to Si (*i.e.*, actinolite), of probable metamorphic origin, but the grain size appears to rapidly decrease approaching the upper contact. The rock also contains major amounts of vesicles and minor mafic fragments (Fig. 3). The vesicles are up to 1 cm across and distributed in two distinct horizons, at ~0–10 cm and 20–30 cm below the upper contact, and as patches up to tens of cm in size (Figs. 3A–B). In fresh rock, the vesicles are filled by calcite ± pyrite amygdules. The mafic fragments are up to 5 cm in maximum dimension (Fig. 3B). Whether the fragments are of volcanic or tectonic origin is uncertain because the upper contact and in particular the immediately overlying rocks are significantly deformed (Fig. 3A). Whether the BCF is of extrusive or intrusive origin is significant in any discussion of its geology. Stone *et al*. (1987, 1995a) have discussed this question and favor its emplacement as a flow. Recently, Houle *et al*. (2004) have presented field observations mainly from along the contact area at the stratigraphic top of the BCF leading to an interpretation that the unit is a high-level sill. Resolution of this question will require careful consideration of effects of deformation along the upper BCF contact and is beyond the scope of the present contribution.

### *Random spinifex zone*

A 5-m-thick zone of randomly oriented spinifex (sample #2) is in gradational contact with the chilled margin (Fig. 2). The random texture is defined by isolated, acicular and fan-like sheaves (up to 20 modal

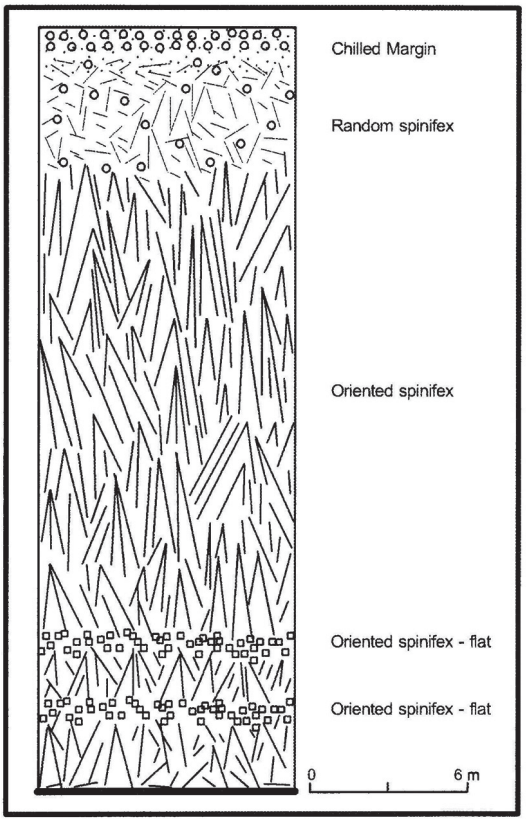


FIG. 2. A stratigraphic section of the spinifex-textured clinopyroxenite layer along Transect 2 of the Boston Creek ferropicrite.

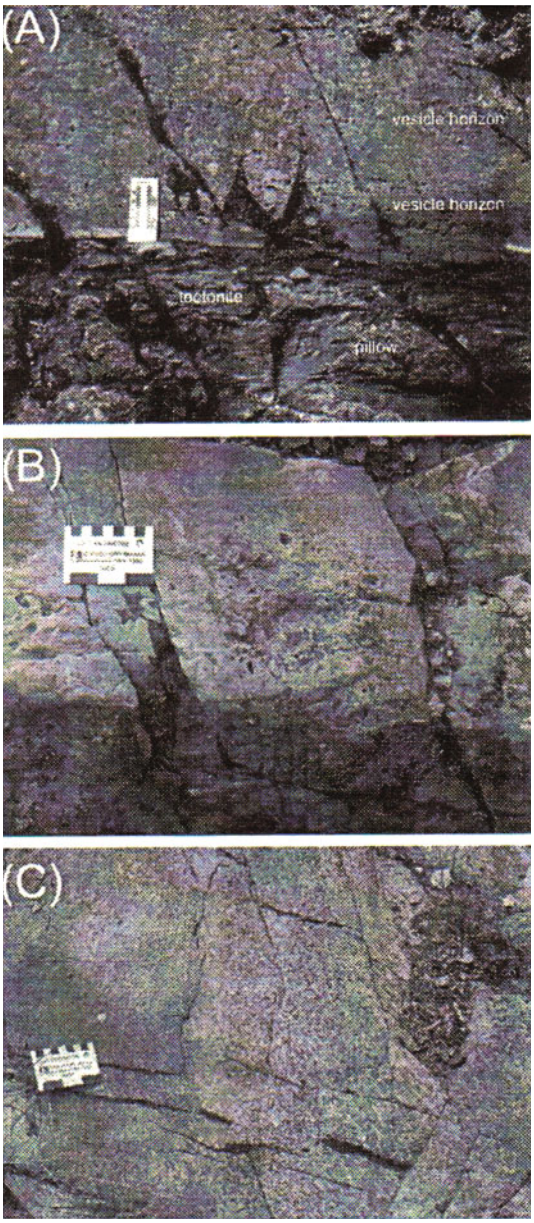


FIG. 3. Outcrop petrography of the chilled margin zone and random spinifex zone of the spinifex-textured layer along Transect 2 of the Boston Creek ferropicrite. (A) Vesicles are distributed in two horizons (delineated by the dashed lines) below the upper contact. The photograph was taken facing west (down section), and the scale is 20 cm in maximum dimension. Note that the chilled margin is overlain by a tectonite (sheared chert?) and pillow basalt. (B) A spherical patch of vesicular material immediately underlying the upper contact. The scale is 8 cm in maximum dimension. (C) Random spinifex, located ~1–3 meters down-section of the upper contact.

% and <50 mm in length) of micro- to macrospinifex clinopyroxene pseudomorphs in an altered, originally glassy groundmass (Fig. 3C). The clinopyroxene grains are completely altered to amphibole. Chromite occurs as small euhedral grains. Vesicles are present locally and filled by calcite ± pyrite. The clinopyroxene grains are larger, more subparallel in orientation and fan-like in arrangement approaching contact with the underlying oriented spinifex zone.

*Oriented spinifex zone*

The oriented spinifex zone, the thickest zone of the spinifex layer, is in gradational contact with the overlying random spinifex textured zone (Fig. 2). The rock consists of huge fan-like sheaves of optically continuous, hollow clinopyroxene grains (10 or more in number, now converted to amphibole) up to 5 mm wide and 50–100 cm long or longer, which are oriented roughly perpendicular to and convex toward the upper contact. Small-scale kinks and folds are apparent locally, though whether such features are relict igneous or deformational remains to be determined. Despite the conversion to amphibole, relict igneous clinopyroxene is well preserved (Fig. 4). The groundmass is skeletal titaniferous magnetite (tree and bug shapes), plagioclase, primary amphibole (Stone *et al.* 2003), altered glass and, at the top, chromite. Vesicles in the form of calcite amygdules are present in minor amounts in the interstices of the spinifex crystals of clinopyroxene. Some of the vesicles appear to have a pipe-like geometry.

In addition, two 1-m-thick zones of distinctly different material are present in the basal 10 m of the oriented spinifex zone (Fig. 2). Initially, these zones were considered to be internal random spinifex. However, closer inspection suggests that they are composed of oriented spinifex grains, but the orientation is subparallel rather than perpendicular to layering, and with steep plunges such that outcrop exposures of the grains are cross-sections. Compared to the majority of the oriented spinifex, these two zones have lower modal abundances of clinopyroxene relative to plagioclase, but they have not been studied in detail. Similar zones have been observed in the basal part of the spinifex layer at Transect 1 and warrant follow-up study.

The basal few meters of the oriented spinifex zone consist of shorter, stubbier, and more closely packed and less uniformly oriented grains of clinopyroxene (Fig. 2). At the base of the spinifex layer, immediately overlying the gabbro, clinopyroxene grains are locally oriented subparallel to the contact and with shallow plunges. The contacts of the oriented spinifex zone with the underlying layer of gabbro are sharp but undulatory at the meter scale along strike.

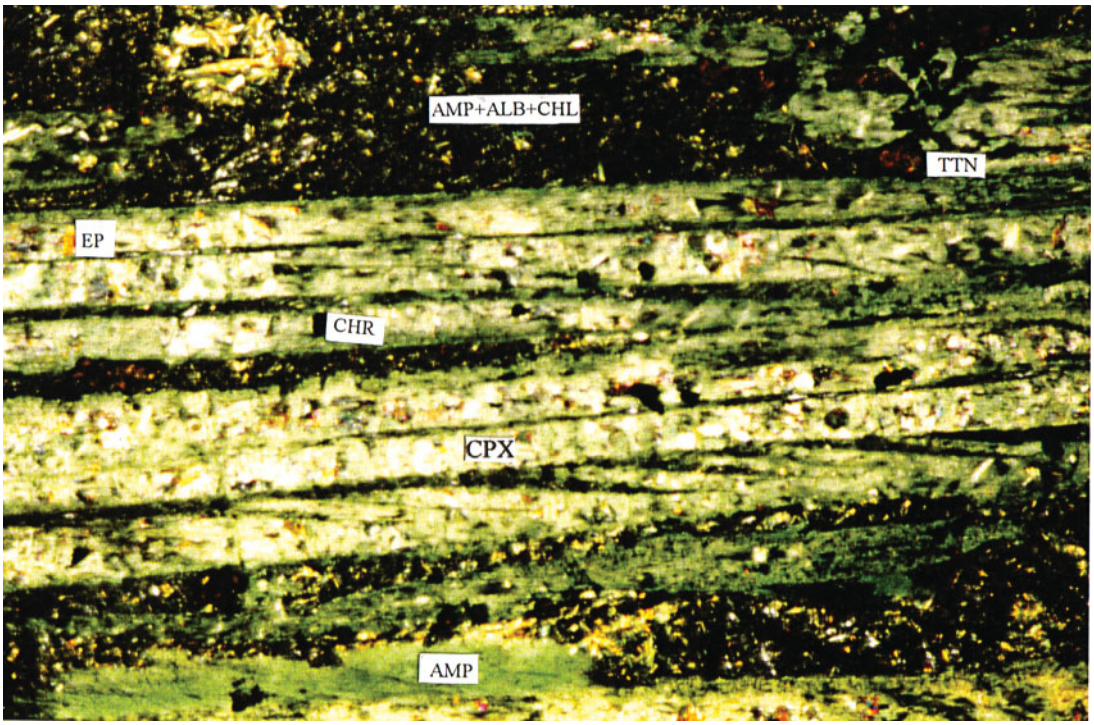


FIG. 4. Petrography of the oriented spinifex zone. Photomicrograph of relict spinifex clinopyroxene [CPX, light green with white (ALB) patches] and replacement amphibole alteration (AMP, grey). Symbols: EP: epidote, ALB: albite, CHL: chlorite, TTN: titanite, CHR: chromite (black).

## COMPOSITION OF CLINOPYROXENE OF THE SPINIFEX LAYER

### *Spinifex clinopyroxene*

Stone *et al.* (1987, 1995a) established the Ca-rich nature of three samples of spinifex clinopyroxene from Transect 1, some 60 m northwest of Transect 2 (Fig. 1). In Transect 2, fresh clinopyroxene occurs from 13 to 30 m in depth, but is more common in the basal 10 m. The spinifex clinopyroxene grains are altered internally and marginally to amphibole (actinolite, Fig. 4). Spot electron-microprobe analyses were performed on fresh cores and rims, domains indistinguishable by optical properties.

Average compositions for core and rim areas of spinifex clinopyroxene are presented in Table 1. They are plotted in the pyroxene quadrilateral (Fig. 5) in terms of wollastonite – enstatite – ferrosilite (Wo–En–Fs) end-members (Lindsley & Andersen 1983) using the nomenclature of Morimoto (1989), and compared along stratigraphic profiles in Figure 6. The spinifex clinopyroxene plots predominantly as Ca-rich augite with increasing ferrosilite component in the rim (Fig. 5).

Core and rim compositions differ little in the 13–21 m interval, whereas larger variations characterize the 22–30 m interval (Fig. 6). Magnesium is usually depleted in the rim compared to the core, and the converse applies to Fe, resulting in lower Mg# in the rim. The variations in Mn are similar to those for Fe, but the rim enrichments are much larger. The average difference for samples #20 and #22 is 70% MnO, compared with 6% FeO (percentages with respect to core values). The rim-to-core behavior of Cr reverses from 13–21 m where the rim is higher in Cr, to the 22–30 m level, where it is lower, with depletion in the rim of up to 50%.

Core-to-rim variations for other elements in the basal third (#18 to 24) of the spinifex layer are more diverse. Profiles for $SiO_2$, $Al_2O_3$ and $TiO_2$ (Fig. 6) show small (<1 wt%) core-to-rim variations. The $Al_2O_3$ and $TiO_2$ profiles are similar. Whereas cores may be higher or lower than rims from one sample to the next, the sense of the difference is the same for both elements in a given sample. Samples with higher concentrations of Al and Ti in the rim have lower contents of Si in the rim. Core and rim contents of Ca differ by only 0.20 ± 0.04 wt% CaO.

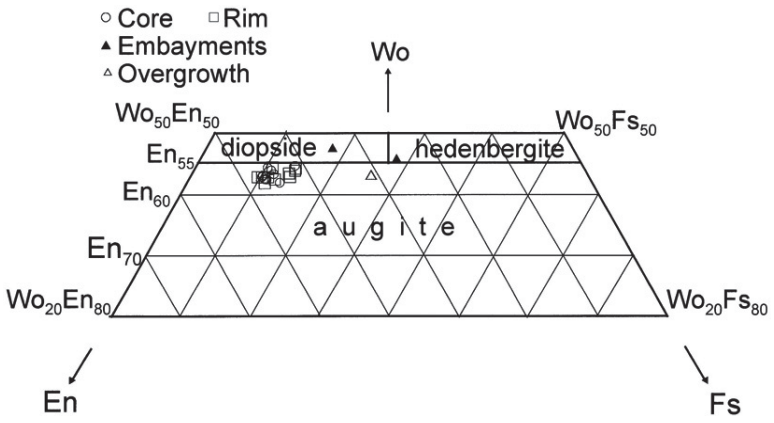


FIG. 5. Clinopyroxene compositions in the pyroxene quadrilateral (Morimoto 1989) illustrating the enrichment of the ferrosilite component in rim domains of some spinifex clinopyroxene grains and the Fe and Ca enrichment of the clinopyroxene in the embayment and overgrowths.

*Embayment and overgrowth clinopyroxene*

A second, texturally distinct clinopyroxene occurs as an embayment in, or overgrowth on, the spinifex clinopyroxene in samples #20 and 22 (Fig. 7). It is compositionally distinct from the spinifex grains (Tables 1, 2), with higher ferrosilite component and, in the case of the embayment samples, higher wollastonite (Fig. 5). One embayment sample plots in the hedenbergite field, and the other as Fe-rich diopside. Both have higher ferrosilite and wollastonite components than the spinifex grains. The overgrowth sample is a Ca-rich augite with ~10% more ferrosilite than the spinifex grains.

For Mg, Cr, Fe, Mn and Na, consistent behavior is apparent for embayments and overgrowths; levels of Mg and Cr are lower, and levels of Fe, Mn and Na higher, than the core-to-rim range of spinifex grains. These compositional differences may be substantial. For example, FeO in embayments and overgrowths is 2.1 and 1.5 times higher, respectively, than average FeO in cores of spinifex clinopyroxene. For MgO, embayments and overgrowths are 1.9 and 1.3 times lower relative to spinifex clinopyroxene. The largest differences are for Mn, which is enriched in embayments and the overgrowth by 2.6 and 3.2 times relative to spinifex cores.

## WHOLE-ROCK COMPOSITIONAL PROFILES IN THE SPINIFEX LAYER

*Major elements*

Variations in major elements (wt.%), Cr (ppm) and Mg# from top to base of the spinifex layer and the distribution of essential and accessory minerals are shown in Figure 8. Distinctive features of whole-rock composition are: a) anomalously high or low concentrations in sample #1 at the stratigraphic top of the spinifex layer, b) reversals in the compositional trend in the basal 10 m of the section, and c) relatively little compositional variation in the 10–20 m interval. Elements with unusual values in sample #1 include Si, Fe and Ca, with Si lower and Fe and Ca higher than other samples in their respective profiles. For example, $SiO_2$ is 43.0 wt.% compared with an average of 48.7 ± 1.0 wt.% for the rest of the profile. Sample #2, random spinifex 0.9 m below sample #1, has 48.1 wt.% $SiO_2$, close to the profile average. The LOI for #1 is 6.1 wt.%, significantly exceeding the profile average, 1.9 ± 1.0%. Stone *et al.* (1995b) demonstrated a gain in Ca at the top of the spinifex layer along Transect 1.

Compositional reversals are conspicuous for MgO, $Al_2O_3$, $Na_2O$ and Mg# in the basal 10 m (Figs. 8A, B). Profiles for MgO, Mg#, $Cr_2O_3$ and CaO are broadly convex toward lower concentrations with minima at 25 m, whereas $Al_2O_3$ and $Na_2O$ peak toward maximum concentration at or near 25 m. Although sample-to-sample compositional variation is large by comparison with the total variation of a given profile, $SiO_2$, FeO and MnO vary systematically down section if sample #1 is excluded. Linear fits (not shown) indicate increasing $SiO_2$ and decreasing FeO and MnO with depth.

*Compatible elements*

Compositional profiles for Ni, Co and Cr (Fig. 8C) show progressive depletion from the stratigraphic top to ~2 m depth in the spinifex layer. This trend is comparable to that of MgO, although the MgO depletion

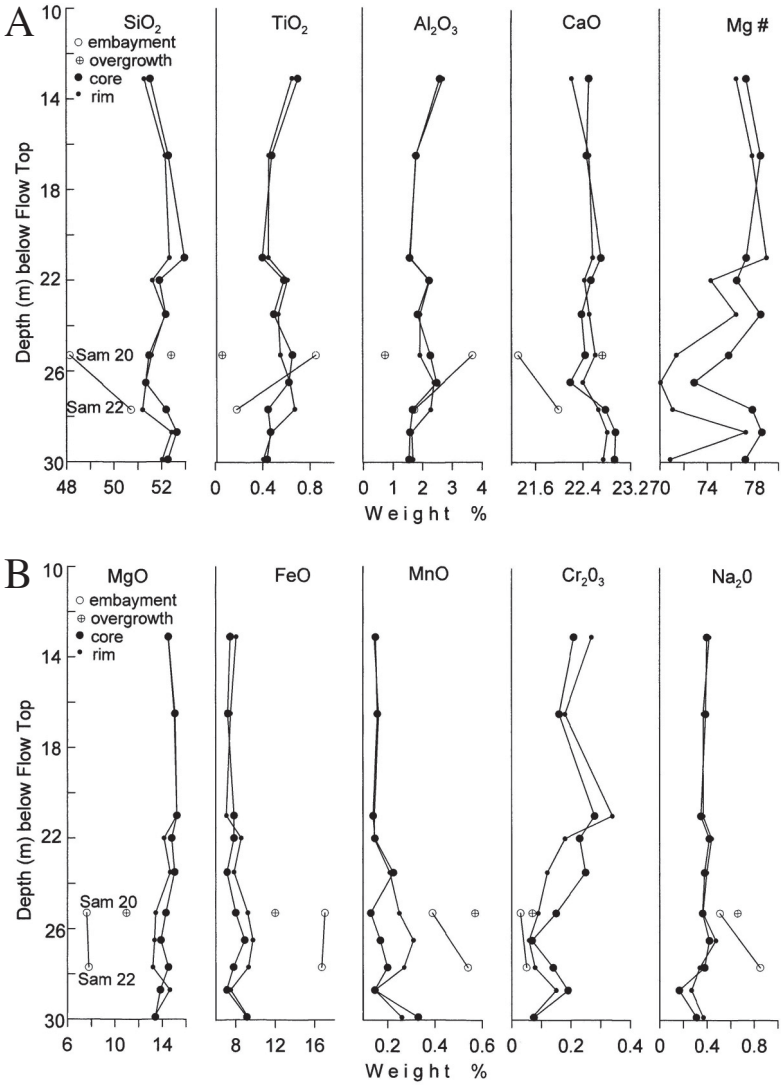


FIG. 6. Comparison of core and rim compositions of spinifex clinopyroxene and of embayment and overgrowth clinopyroxene from the spinifex-textured layer of the Boston Creek ferropicrite, in terms of major and minor elements. (A) Contents of $SiO_2$, $TiO_2$, $Al_2O_3$ and values of Mg# *versus* depth in the spinifex-textured layer. (B) Contents of MgO, FeO, MnO, $Cr_2O_3$ and $Na_2O$ *versus* depth.

extends to ~5 m. Clinopyroxene–basalt partition coefficients for these trace constituents vary from 1.2 for Co to 10 for Cr (Dostal *et al*. 1983, Grove & Bryan 1983). Hence, compatible behavior is a likely cause of the depletion trends near the top of the spinifex layer. Little variation in MgO, Cr or Ni is evident in the 10–20 m depth range, but distinct reversals in trend occur below 20 m for MgO and Cr.

*Incompatible elements*

Profiles for U, Th, Ta, Nb, Zr, Hf, LREE and HREE (Fig. 8D) illustrate the highly coherent behavior of these elements. For fractionation between clinopyroxene and basaltic melt, partition coefficients range from approximately 0.01 to 0.70 (Dostal *et al*. 1983, Rollinson 1993), implying preferential partitioning into the melt. Rela-

tively small changes in concentration of one element are commonly shown by the entire suite. For example, samples #6, 10 and 19 have either higher or lower concentrations relative to their nearest neighbors with regard to all the elements. This probably reflects whole-rock concentrations governed mainly by differences in amount of trapped interstitial melt at different stages in the growth of the spinifex layer.

*Siderophile and chalcophile elements*

Variations in PGE, Au, Cu and S across the spinifex layer (Fig. 9) represent a complete dataset for Pt and Pd and a subset including sample #1 and the even-numbered samples for the other PGE. The Ir profile is constrained by concentrations of seven samples at the detection limit of 0.1 ppb. Nevertheless, the most significant feature of the profiles, increases in concentration at 20 m depth, is clearly shown by the Ir data.

Relatively high concentrations of these elements occur at the top of the spinifex layer and at 20 m (sample #16). The highest concentration of each element is at the top of the spinifex layer (sample #1, chilled margin) except for Ru, where the highest value is at the base of the spinifex layer (sample #24). For Au and S, enrichment in the chilled margin (sample #1) is 280 and 8 times higher, respectively, than the profile average. Whereas Pd, Pt and Rh are only slightly higher in the chilled margin relative to the profile average (1.7, 1.3 and 1.5 times, respectively), Ir and Ru are 4.3 and 3.2 times higher (ignoring Ru in sample #24). The higher content of siderophile and chalcophile elements (PGE, Ni, Co) as well as MgO and Cr at the top of the spinifex layer (samples #1 and 2), together with the fine-grained texture of sample #1, strongly suggest that these samples represent the closest approximation to parental magma compositions. Especially significant is the high content of both iridium-group PGE (IPGE: Ir and Ru) and platinum-group PGE (PPGE: Rh, Pt and Pd), which indicate a strong inheritance from the mantle. Specifically, the average Pd/Ir value for samples #1 and 2 is 18 compared with 46 for the rest of the spinifex layer. For the primitive mantle of McDonough & Sun (1995), the Pd/Ir value is 1.2.

The top of the spinifex layer is marked by a high LOI of 6.1 wt.% indicative of the $H_2O$, sulfur and carbon contents of the sample. Contamination from wallrocks, outgassing of the BCF with cooling, or some combination of these processes may account for the high LOI. For S, the only constituent actually measured, a very high concentration (11,700 ppm) occurs at the top of the spinifex layer. It is useful to note the implications of the S:Se ratio, a parameter that can have discriminatory value in distinguishing S of magmatic origin from that of sedimentary and hydrothermal sources. Keays & Lightfoot (1999) cited a S/Se value of 3500 as typical of magmatic sulfides and noted that much higher values may characterize sedimentary sulfides. Ignoring samples #4 and #7 at the Se detection limit of 0.1 ppm (Table 3), the average S/Se value for the BCF spinifex layer is 4000 ± 2700, favoring a mainly magmatic origin for S. In addition to the S:Se ratio, the occurrence of magmatic $H_2O$ in the BCF (Stone *et al*. 2003) and the presence of calcite-bearing vesicles near the top of the spinifex layer (Stone *et al*. 1995a) tend to support outgassing as a significant contributor to the high LOI at the top of the BCF. Significant fractionation of PGE due to the high LOI is deemed unlikely.

Comparison of profiles (Fig. 9) shows that most PGE and chalcophile elements have higher concentrations at 20 m (sample #16), a feature obvious for Ir, Ru, Rh, Pd, Cu and S, but weak for Pt. Using the ratio [sample #16/(nearest neighbor average)] as a ranking index, the magnitude of profile peaks at 20 m is Ru > Pd > Ir = Cu

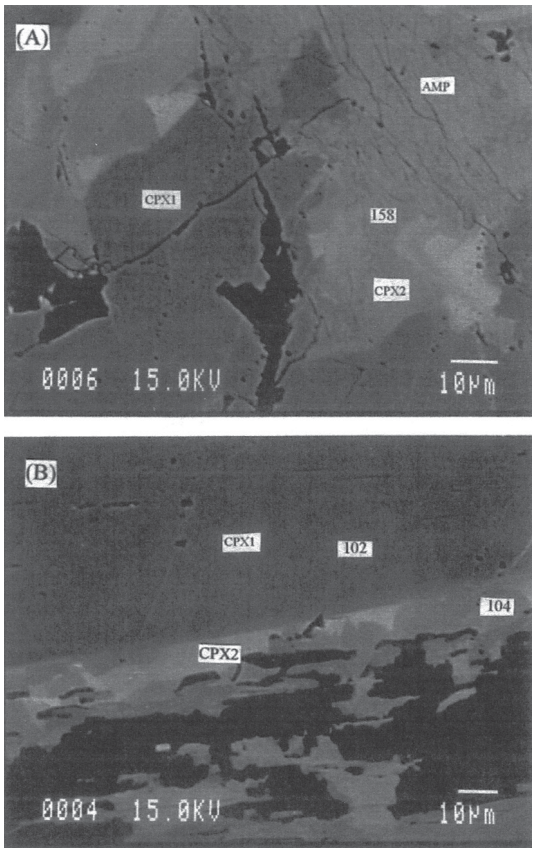


FIG. 7. Petrography of the embayment and overgrowth clinopyroxene. (A) Back-scattered-electron image of clinopyroxene (CPX2) in an embayment relationship with spinifex clinopyroxene (CPX1, dark). (B) Back-scattered-electron image of overgrowth clinopyroxene (CPX2) at the margin of spinifex clinopyroxene (CPX1).

> Rh > S > Pt, where the peak-to-nearest-neighbor ratio varies from 4.0 for Ru to 1.2 for Pt (Table 3).

A mantle-normalized plot of PGE, Ni and Cu (Fig. 10) shows the unique character of the stratigraphic top of the spinifex layer, which has the highest content of PGE, Ni and Cu, and contrasts the compatible behavior of Ir with the mainly incompatible behavior of the other PGE. Thus, Ir is depleted in most of the spinifex layer relative to the chilled margin and random spinifex, indicating that the depletion occurred in the earliest stages of crystallization. In contrast, other PGE are higher than in random spinifex, which indicates increasing concentration in the magma with progressive crystallization.

### *Correlations*

Correlations among the elements are presented as Pearson's r coefficients in Table 4 and are calculated for 22 samples, except for Ir, Ru, Rh and Au, where the database is 12 samples. Sample #1, from the chilled margin, was omitted because of uncertain implications of the high LOI. The significance of r values was tested against the Student's t distribution. Except for Ir, Ru, Rh and Au, r values represent highly significant correlations at a 0.1% probability level; that is, the discriminant value of Student's t will be exceeded by chance once in 1000 trials. The discriminate r value for this probability level is 0.65. In the case of the smaller Ir–Ru–Rh–Au database, the discriminant r value for a 0.1% probability level is 0.82 (correlation is highly significant), and for a 1% probability level, it is 0.71 (correlation is significant). The strongest correlations for the PGE subset (Table 4) are between the 1 and 0.1% probability levels (*i.e.*, $r \geq 0.71$ but $< 0.82$).

Interelement correlations were determined for all elements in Table 4, but only those with at least one r value significant at an 0.1% level ($r \geq 0.65$), or in the case of the Ir–Ru–Rh–Au subset, at a 1% level ($r \geq 0.71$), are presented in Table 4. A notable aspect of the PGE correlations is the strong positive correlation of Pt with FeO, $TiO_2$ and U, for which $r \geq 0.65$, implying

TABLE 4. CORRELATION COEFFICIENTS (PEARSON'S R) FOR WHOLE-ROCK MAJOR AND TRACE ELEMENT CONTENTS IN THE BOSTON CREEK FERROPICRITE LAYER

| | $SiO_2$ | $Al_2O_3$ | FeO | MgO | CaO | $Na_2O$ | $K_2O$ | $TiO_2$ | Mg# | Cr | Zn | V | Sc | Ba | Sr | LREE | Eu | HREE | U | Zr | Hf | Co | Ni | Ir | Ru | Rh | Pt | Pd | Au | As | S |
|---|---|---|---|---|---|---|---|---|---|---|---|---|---|---|---|---|---|---|---|---|---|---|---|---|---|---|---|---|---|---|---|
| $SiO_2$ | | | | | | | | | | | | | | | | | | | | | | | | | | | | | | | |
| $Al_2O_3$ | | | | | | | | | | | | | | | | | | | | | | | | | | | | | | | |
| FeO | -0.80 | | | | | | | | | | | | | | | | | | | | | | | | | | | | | | |
| MgO | | -0.77 | | | | | | | | | | | | | | | | | | | | | | | | | | | | | |
| CaO | | | | | | | | | | | | | | | | | | | | | | | | | | | | | | | |
| $Na_2O$ | | 0.81 | -0.91 | | | | | | | | | | | | | | | | | | | | | | | | | | | | |
| $K_2O$ | | 0.75 | -0.65 | | | | | | | | | | | | | | | | | | | | | | | | | | | | |
| $TiO_2$ | | | | | | | | | | | | | | | | | | | | | | | | | | | | | | | |
| Mg# | | -0.88 | 0.91 | | -0.82 | -0.73 | | | | | | | | | | | | | | | | | | | | | | | | | |
| Cr | | | 0.79 | | -0.73 | | | 0.66 | | | | | | | | | | | | | | | | | | | | | | | |
| Zn | | | | | -0.67 | | | | | | | | | | | | | | | | | | | | | | | | | | |
| V | | | | | | | | 0.67 | | | | | | | | | | | | | | | | | | | | | | | |
| Sc | | -0.69 | | 0.66 | | | | | | | | | | | | | | | | | | | | | | | | | | | |
| Ba | | | -0.65 | | 0.76 | 0.71 | | | | | | | | | | | | | | | | | | | | | | | | | |
| Sr | | | -0.78 | | 0.80 | | | -0.72 | -0.65 | | | | | | | | | | | | | | | | | | | | | | |
| LREE | | 0.83 | -0.82 | | | 0.72 | | -0.90 | | | | | | | | | | | | | | | | | | | | | | | |
| Eu | | 0.73 | | | | 0.68 | | -0.71 | | | | | | | | 0.70 | | | | | | | | | | | | | | | |
| HREE | | 0.84 | -0.70 | | | 0.82 | 0.69 | -0.83 | | | | | | | | 0.87 | 0.73 | | | | | | | | | | | | | | |
| U | | 0.77 | | | | 0.71 | 0.66 | -0.74 | | | | | | | | 0.82 | 0.79 | 0.88 | | | | | | | | | | | | | |
| Zr | | 0.84 | | | | 0.83 | | -0.81 | | | | | | | | 0.82 | 0.73 | 0.93 | 0.90 | | | | | | | | | | | | |
| Hf | | 0.79 | -0.67 | | | 0.79 | 0.68 | -0.84 | | | | | | | | 0.82 | 0.73 | 0.94 | 0.90 | 0.95 | | | | | | | | | | | |
| Co | | | 0.69 | | -0.69 | | | | 0.67 | 0.67 | | | | | | | | | | | | | | | | | | | | | |
| Ni | | -0.66 | 0.85 | | -0.74 | | | 0.72 | 0.83 | 0.66 | | | | | | -0.74 | | -0.71 | | | | 0.82 | | | | | | | | | |
| Ir | | *-0.73* | *0.76* | | *-0.71* | | | *0.75* | | | | | | | | | | | | | | | | | | | | | | | |
| Ru | | | | | | | | | | | | | *0.78* | | | | *-0.84* | | | | | | | | | | | | | | |
| Rh | | | | | | | | | | | | | | | | | | | | | | | | | | | | | | | |
| Pt | | | 0.67 | | | | | 0.74 | | | | | | | | | | | 0.71 | | | | | | | | *0.76* | | | | |
| Pd | | | | | | | | | | | | | | | | | | | | | | | | | | | | | | | |
| Au | | | | | | | | | | | *0.65* | | | | | | | | | | | | | | | | | | | | |
| As | | | | | | | | | 0.68 | | | | | | | | | | | | | | 0.82 | | | | | | | | |
| S | | | | | | | | | | | | | | | | | | | | | | | | | | | | | | | 0.67 |

For all correlations except the PGE, $r \geq 0.65$ is highly significant, 0.1%. For Ir, Ru, Rh and Au (r values italicized, $r \geq 0.82$ is highly significant, 0.1%, and $r \geq 0.71$ is significant, 1%.

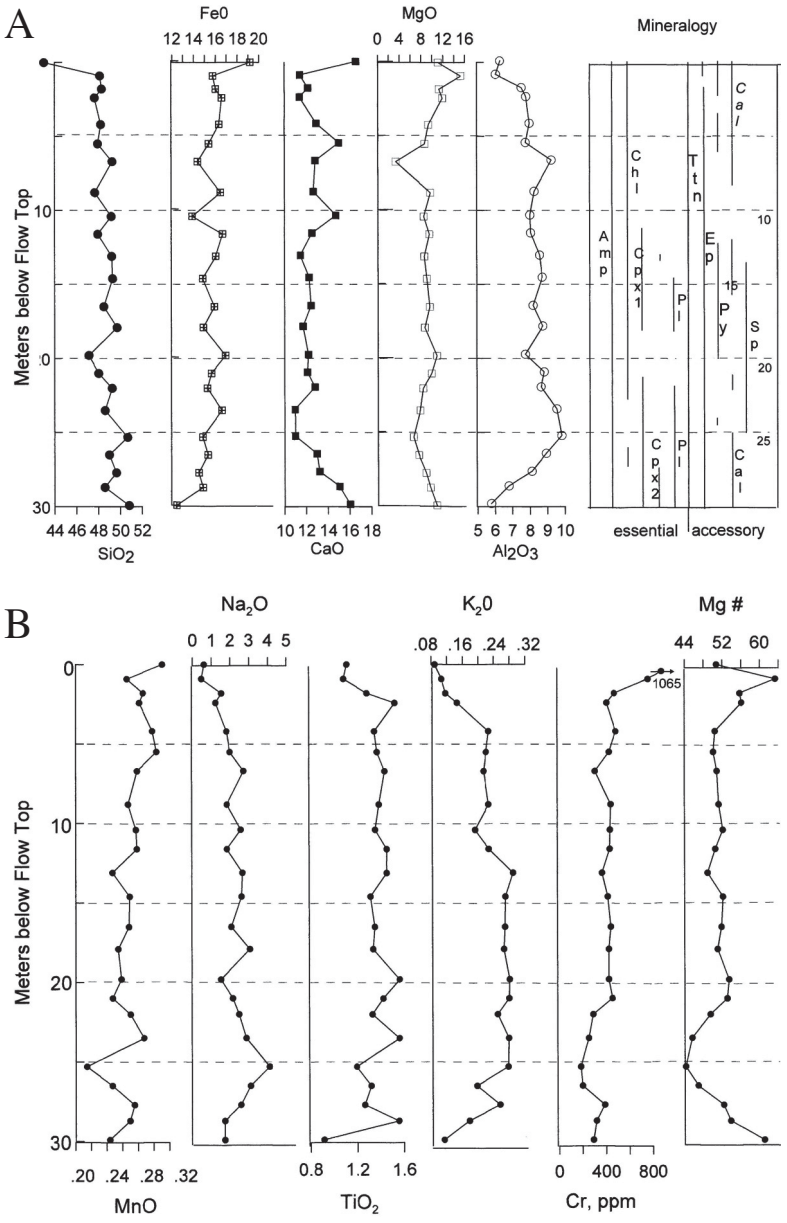


FIG. 8. Variations in whole-rock geochemical composition with depth in the spinifex-textured layer. (A) Stratigraphic profiles of $SiO_2$, CaO, $Al_2O_3$, FeO and MgO variations. (B) Profiles of MnO, $TiO_2$, Cr, $Na_2O$ and $K_2O$ across the spinifex layer. (C) Profiles of MgO, Cr, Ni and Co variations. (D ) Profiles of highly incompatible elements. Symbols: Act: actinolite, Chl: chlorite, Cpx1: spinifex clinopyroxene, Cpx2: embayment and overgrowth clinopyroxene, Pl: plagioclase, Ttn: titanite, Ep: epidote, Py: pyrite, Cal: calcite, and Sp: spinel.

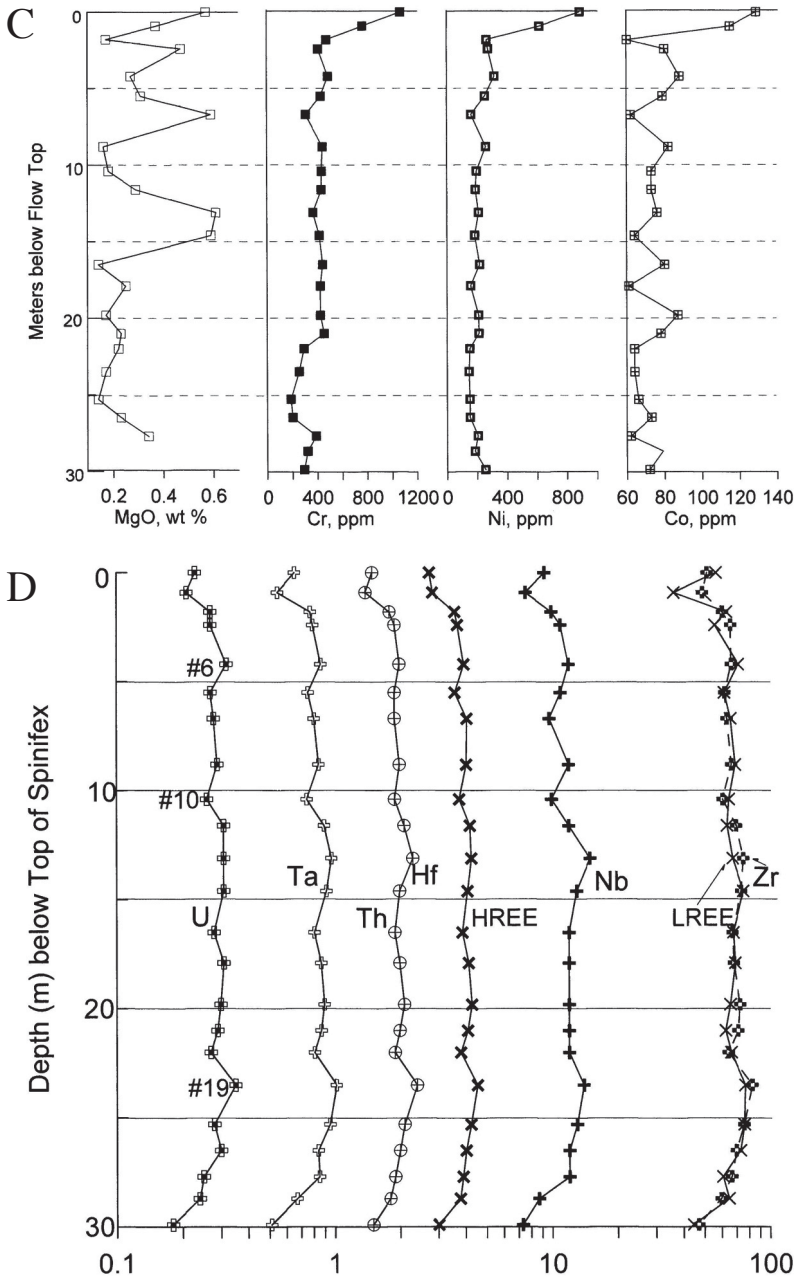


a highly significant correlation. The level of platinum also correlates positively with that of Rh, where $0.71 < r < 0.82$ indicates a significant correlation at a 1% or better significance level. The correlations of Pt with FeO and $TiO_2$ suggest sensitivity to oxygen fugacity, whereas the correlation with U reflects incompatible behavior. The coherence of Rh and Pt suggest that Rh is probably partitioned mainly into melt. None of the correlations exhibited by Pt are observed for Pd. The highly incompatible elements U, Zr, and Hf show strong positive correlation with the REE, Na and K.

*Comparison of whole-rock and clinopyroxene profiles*

Whole-rock profiles are compared with those of the average core of the spinifex clinopyroxene in Figure 11.

In principle, variations in magma composition and site preferences dictated by the clinopyroxene structure may influence clinopyroxene composition. For Si, Ca, Fe and Mg, the mineral and whole-rock profiles show little similarity on a sample-to-sample basis. Where whole-rock profiles show distinctive compositional reversal of Mg and Ca in the basal 10 meters, there is no comparable change in clinopyroxene composition. For the minor constituents Al, Ti, Mn, Na and Cr, there is significant parallelism only for Mn. For other minor elements, variations in pyroxene composition do not correlate with whole-rock composition. Marked trends such as the compositional reversal of Na are not reflected in the pyroxene composition.

## Growth History of the Clinopyroxene

The origin of the spinifex pyroxene texture has been considered by Arndt & Fleet (1979), Campbell & Arndt (1982), Donaldson (1982), Barnes *et al*. (1983), Kinzler & Grove (1985), Stone *et al*. (1995a), Shore & Fowler (1999) and Arndt & Fowler (2004), with a focus on spinifex olivine in komatiites. The consensus is that strong directional supercooling generates spinifex clinopyroxene. Campbell & Arndt (1982) interpreted experimental studies to indicate that spinifex clinopyroxene crystallized metastably from supercooled melts. Alternatively, Kinzler & Grove (1985) argued from their experimental studies that pyroxene spinifex will crystallize only after removal of olivine from supercooled magma subjected to prior crystallization of olivine. They also contended that for komatiitic melts, initial crystallization of pyroxene is dependent on composition of parental magma. For the BCF, Stone *et al*. (1995a) argued that higher Ca, Fe and Mg relative to Al in comparison with mafic rocks at similar MgO content, as well as high volatile content in the parental melt (Stone *et al*. 2003, 2005), are factors that would increase the interval of spinifex clinopyroxene crystallization.

### *Primary magmatic clinopyroxene*

Although relict spinifex clinopyroxene is absent in the upper 13 m of the spinifex layer, distinct patterns of core-to-rim variation characterize the lower two-thirds of the spinifex layer. The most obvious contrast is the very small core-to-rim difference in the middle

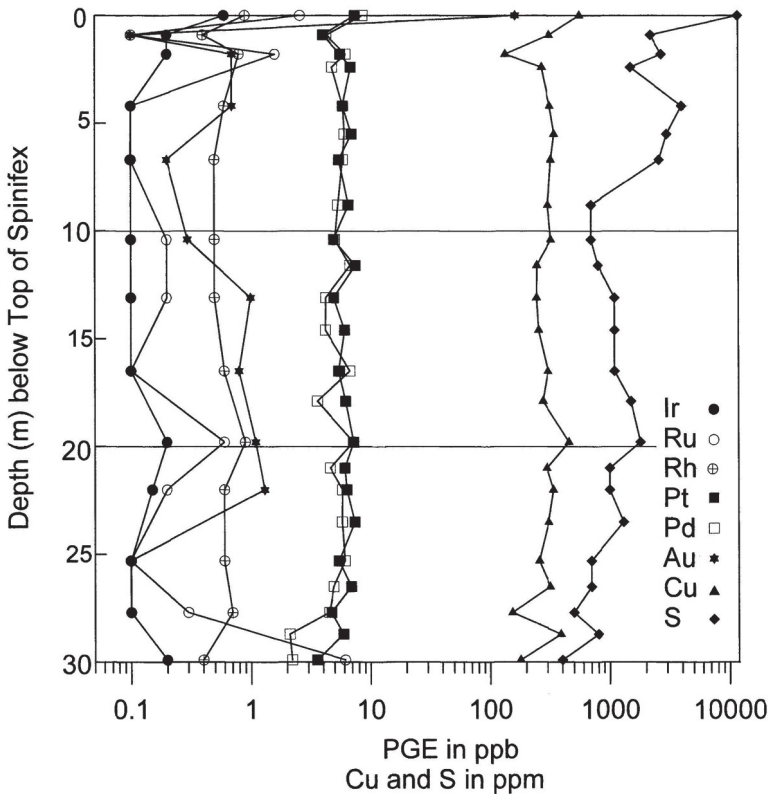


FIG. 9. Stratigraphic profiles of PGE–Cu–S for the spinifex-textured layer.

third compared with the much larger differences in the bottom third of the layer. The most systematic variation in the 22 to 30 m depth-range is the Fe enrichment in the rim and the complementary Mg depletion, with an average increase in FeO content of rims by 10 wt.% relative to the core average. Large differences in core-to-rim concentrations characterize Cr and Mn. The former is higher in rims by 20% on average at 20 m and above, but lower by 30% from below this level to the base of the spinifex.

Partition coefficients are useful parameters indicative of the direction of element partitioning (into the melt if $D < 1$ and into the solid phase if $D > 1$) as equilibrium is approached. For Cr, values of 34 and ≥10 (Dostal *et al*. 1983, Grove & Bryan 1983, respectively) imply strong magmatic fractionation of Cr into pyroxene, but the significance of temperature has not been constrained experimentally. Further, Cr partition will be influenced by whether chromian spinel is on the liquidus. In any case, reaction of clinopyroxene with interstitial melt appears to reverse with progressive fractional crystallization. An average Mn enrichment of 70% in clinopyroxene rims is observed in three of five samples (#20, 21 and 22) in the basal 5 m of the spinifex layer. Experimental partition-coefficients for Mn between diopsidic pyroxene and mafic silicate melt vary from 0.3 to 1.2, increasing with decreasing temperature from 1300 to 1170°C (Lindstrom & Weill 1978). Hence, Mn should not partition strongly into clinopyroxene at magmatic temperatures, but would do so more strongly with decreasing temperature. The average Mn content in embayment and overgrowth clinopyroxene is three times that of the spinifex clinopyroxene. This may reflect an increase in the partition coefficient with decreasing temperature or a reaction with late-stage magmatic fluids of different composition than gabbro-stage magma.

Core-to-rim variations in Si average ~1 wt.% over the 22–30 m depth, with lower concentrations of Si characteristic of the rim domain. The profiles of Si and Al are complementary in that high values of one constituent in the core are matched by low values of the other on a sample-by-sample basis. The Ti profile is similar to that of Al and exhibits the same relationship with Si, which suggests substitution of Al and Ti for Si (Fleet 1974, Lindsley & Andersen 1983, Morimoto 1989).

Processes that could generate core-to-rim compositional variations include those of essentially magmatic character, or postmagmatic processes involving metamorphism and metasomatism. A magmatic control would include interaction between primary spinifex-textured clinopyroxene and trapped interstitial melt,

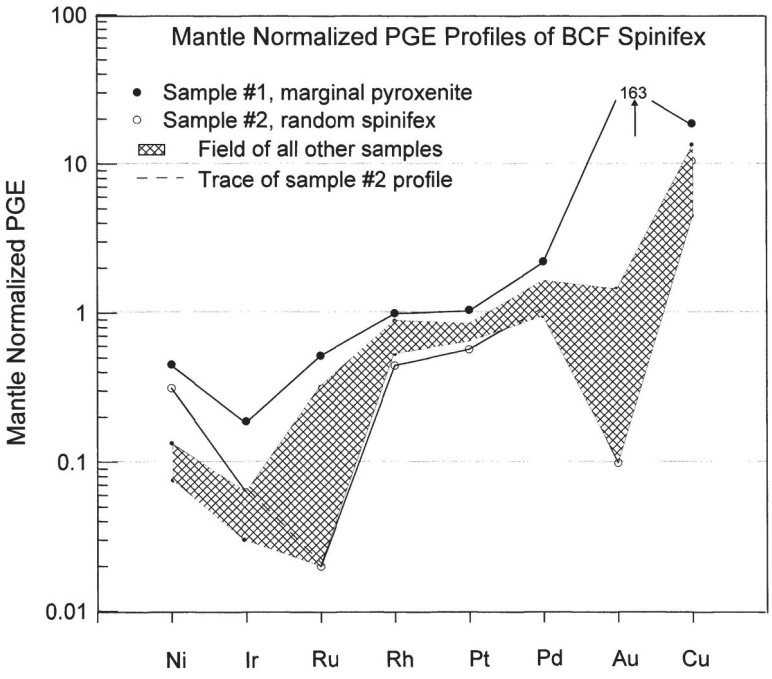


FIG. 10. Mantle-normalized PGE profiles illustrating compatible behavior of Ir and Ru, and incompatible behavior of Pt, Pd and Rh. The mantle-normalization values are from McDonough & Sun (1995).

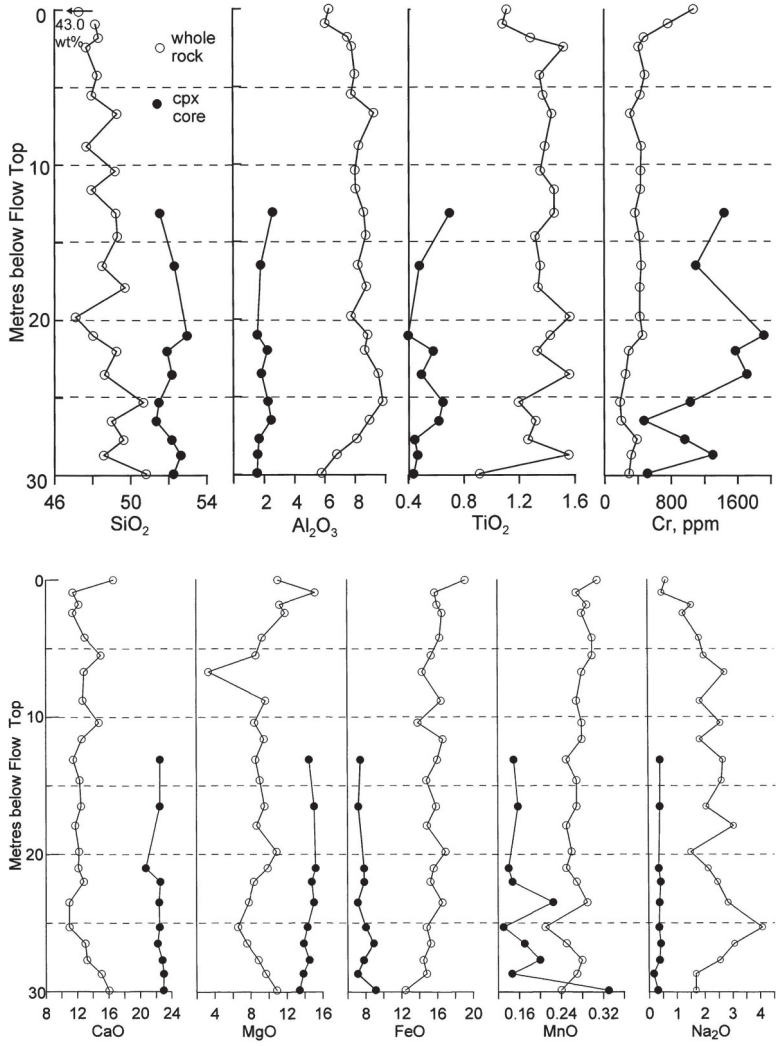


FIG. 11. Comparison of compositions of whole rocks and of the core of spinifex clinopyroxene along the stratigraphic profile. (A) Plot of contents of $SiO_2$, $Al_2O_3$, $TiO_2$, and Cr *versus* depth in the spinifex-textured layer. (B) Plots of contents of CaO, MgO, FeO, MnO, and $Na_2O$ *versus* depth.

with the clinopyroxene laths regarded as cumulus phases in the sense proposed by Campbell & Arndt (1982), and the interstitial melt an intercumulus liquid. Much as in the case of layered intrusions, a variety of reactions between these two domains can be anticipated. Such interaction will be facilitated by exchange processes occurring at high magmatic temperatures and, in the case of the BCF, by high content of magmatic $H_2O$ content (up to 2 wt.%, Stone *et al*. 2003), as well as changing composition of the melt in response to fractional crystallization, which ultimately generated the four major layers of the BCF. As suggested subsequently, if injection of fresh magma has occurred, changes in compositional and thermal parameters of interstitial melt can be expected. The groundmass texture in the spinifex layer is very fine-grained in general and suggestive of high rates of cooling that could limit the extent to which exchange reactions with the clinopyroxene-trapped melt can occur.

The metamorphic history involves a regional grade of pumpellyite–prehnite facies (Jolly 1980) with a significant tectonic and contact-metamorphic overprint imposed some 30 Ma after emplacement of the BCF (2720 ± 2 Ma; Corfu & Noble 1992) as a consequence

of the intrusion of the Round Lake Batholith (~2690 Ma; Corfu *et al*. 1989). The primary magmatic mineralogy of the BCF has been extensively modified by metamorphism (Stone *et al*. 1987). In the spinifex layer, nearly pervasive replacement of clinopyroxene by amphibole (actinolite) has occurred in the upper 15 to 20 m of the layer, although with preservation of spinifex texture. Such alteration is less intense in the basal 10 to 15 m of the layer, but marginal zones of relict magmatic clinopyroxene are commonly mantled with actinolite. Although rare, primary magmatic amphibole (magnesiohastingstite) occurs in the groundmass in the basal 10 m of the layer (Stone *et al*. 1987, 2003). The extensively altered state of the BCF prompts consideration of metamorphism as an alternative factor responsible for core-to-rim variation in spinifex-textured clinopyroxene. Whereas we favor the magmatic option, the possibility that such compositional variation is induced by metamorphic gradients cannot be ruled out.

Mobility of Ca and $H_2O$ and the introduction of $CO_2$ are implied by the alteration assemblages. However, the unusual composition of the BCF, including the high levels of Fe, Ti and highly incompatible trace elements and low levels of Al and moderately incompatible trace elements, cannot be explained by significant mass-transfer between the enclosing tholeiitic basalts and the ferropicritic BCF (Stone *et al*. 1996b). Further, although relict igneous clinopyroxene, is metamorphically altered to amphibole throughout the entire BCF, the restriction of the Mn-rich clinopyroxene, as represented by the rim enrichments (Fig. 6B) and the exceptionally Mn-rich overgrowth and embayments, is confined to the basal 5 m of the spinifex layer. The average MnO content of the clinopyroxene in this interval (samples 20 to 24), including the embayment and overgrowth samples and using the core-to-rim average for the spinifex samples, is 0.30 ± 0.15 wt.%. All other MnO values for cumulus clinopyroxene [gabbro and clinopyroxenite layers, including 13 samples from Stone *et al*. (1987, 1993, 1995a)] average 0.19 ± 0.04 wt.%. The restriction of MnO enrichment to a specific layer of the BCF is considered a feature more consistent with a magmatic origin.

An objective discrimination between magmatic and metamorphic scenarios is difficult to make based on the clinopyroxene profiles discussed above. A preference for the magmatic option is held on the basis of a perception that core-to-rim compositional differences are primarily due to exchange reactions between clinopyroxene and interstitial material and that such exchange will occur more efficiently under higher magmatic temperatures than at temperatures associated with an upper greenschist to amphibolite metamorphic regime.

*Postmagmatic clinopyroxene*

The presence of an embayment and overgrowth of spinifex clinopyroxene indicates a later paragenesis for these grains. Minerals in grain-boundary contact with these domains of secondary clinopyroxene are chlorite and amphibole. As hydrous minerals, their association suggests involvement of fluids with significant $H_2O$ content in the origin of the secondary clinopyroxene.

Examples of clinopyroxene with textural attributes indicating a later paragenesis than magmatic pyroxene have been described from the Skaergaard Intrusion and designated hydrothermal clinopyroxene (Manning & Bird 1986). They estimated temperatures of formation between 500° and 750°C, based on clinopyroxene solvus thermometry. A secondary clinopyroxene – chlorite – spinel assemblage in clinopyroxenite of the Mann Complex, Abitibi belt, Ontario was interpreted by Good *et al*. (1997) to be due to hydrothermal alteration at temperatures above 500°C.

The secondary pyroxene in the BCF suite is characterized by higher Fe and, for the embayments, higher Ca contents than spinifex clinopyroxene. It tends to be either higher or lower in a given element than either cores or rims of spinifex clinopyroxene, except for Al and Ti, where a crossover occurs with respect to the primary profile. If there is a fairly consistent trend between core-to-rim differences of magmatic pyroxene, as observed with Mg, Fe, Mn and Cr, the element concentration in the secondary clinopyroxene is in the same sense as the core-to-rim variation in the spinifex clinopyroxene. For example, spinifex clinopyroxene has lower Mg in the rim compared with the core, whereas a rim of even lower Mg characterizes the secondary clinopyroxene. The secondary pyroxene is probably the product of a reaction between primary clinopyroxene and an aqueous fluid during subsolidus cooling at temperatures above 500°C.

*Whole-rock trends*

Whole-rock profiles show maximum compositional variability in the basal 20–30 m and the top 5 m of the spinifex layer, whereas a relatively uniform composition prevails at depths of 5–20 m. Elements compatible in the clinopyroxene structure (mineral/melt D > 1), such as Ni and Cr, are rapidly depleted in the melt, whereas the incompatible elements Al, Ti, Na and K increase with fractional crystallization. Partition coefficients (Rollinson 1993) also indicate a stronger partitioning of Ni and Co into olivine than clinopyroxene, which may explain the relatively strong depletion in Co in that D values for Co partitioning into clinopyroxene are only 0.2–2 as compared with 6.6 for olivine. A more efficient partitioning of Co into olivine supports the contention of Kinzler & Grove (1985) that olivine fractionation is essential for the development of clinopyroxene spinifex.

The chilled margin (sample #1) at the top of the spinifex layer is characterized by very low Si and Al and high Fe, Ca and LOI relative to the random and oriented spinifex zones (Table 3). Stone *et al*. (1987, 1995a)

concluded that the high-Fe, low-Al and high-LREE properties are inherited from a mantle source-region rather than from contamination and alteration. A supporting observation is that the highest concentrations of Rh, Pt and Pd, elements unlikely to be enriched in crustal rocks (Crocket 2002), occur in the chilled margin. Other distinctive properties are the very high Au (12 and 163 ppb), sulfur (1.1 wt.%), Se, As, and Cu. The enrichment of these elements in the stratigraphic top of the spinifex layer might perhaps reflect subsolidus outgassing of the BCF. The average S:Se ratio of the spinifex layer (4000 ± 2700) suggests that the sulfur may well be magmatic. This inference does not preclude a secondary origin for the amygdaloidal pyrite, perhaps during oxidation of precursor sulfide, possibly pyrrhotite, by late magmatic, $H_2O$-rich fluids.

In contrast to the upper and lower regions of the spinifex layer, the 5–20 m depth interval is of relatively uniform composition, which suggests that magma was well mixed and homogenized in this interval. Arndt (1986) has argued for vigorous convection in the crystallization of komatiite flows at Alexo, Ontario (parental magma ≈ 28 wt% MgO). The case for convection in basalt magmas (lower temperature, higher viscosity, parental MgO <15 wt%) is supported (Martin *et al*. 1987) and contradicted (Brandeis & Marsh 1989) in the literature.

The basal 10 m of spinifex are characterized by distinctive reversals in the compositional trends for Mg, Al, Na and Cr, as well as Mg#. An explanation of compositional reversals at the base of the spinifex layer is presented below.

## Magma Recharge

Several lines of evidence point to magma recharge during formation of the gabbro layer within the BCF. The first is the calculation of a fractional crystallization model (Stone *et al*. 1995b, 1996), which demonstrates that PGE concentrations in melts parental to gabbro are too low by almost an order of magnitude to explain the PGE grades observed in the *in situ* sulfide–oxide-hosted mineralization in the gabbro layer. This result suggests an additional flux of unfractionated basaltic magma. The second is the PGE, Cu and S enrichment at a depth of 20 m. The key observation is that all PGE peak together, along with Cu and S. This association of all the PGE suggests that an immiscible sulfide liquid was involved in concentrating these elements. Hence, sulfide of mantle origin, extracted in basaltic partial melts of mantle peridotite, seems the most obvious source of a melt enriched in all the PGE. Except for Rh, PGE concentrations at 20 m are less than in the chilled margin. Lower levels of the PGE are expected because any injection of fresh magma will mix with PGE-depleted residual melt following *in situ* PGE mineralization in the gabbro layer.

The very high and quite different Au contents of the chilled margin (12 and 163 ppb) are from lead and nickel sulfide fire assays on two different 16-gram samples. Discounting significant analytical error, because of good agreement on simultaneously analyzed international reference standards, these values suggest the occurrence of particulate Au in these samples. Whereas alteration and contamination cannot be discounted, carbonate–pyrite-bearing amygdules at the top of the spinifex layer suggest that late or postmagmatic transport of volatiles may have enriched the rock in S, Se and Au.

Additional support for the injection of new magma arises from the Os isotopic systematics (Walker & Stone 2001) and detailed magnetic studies of the BCF (Larson 1994). Whereas an Os/Re isochron (2708 ± 13 Ma) is within statistical uncertainty of the U–Pb baddeleyite age for the BCF (2720 ± 2 Ma; Corfu & Noble 1992), two samples near the top of the gabbro layer, 6–9 m below the base of the spinifex, have highly radiogenic Os, which Walker & Stone (2001) considered indicative of late-stage addition of radiogenic Os from PGE mineralized zones. Whereas the source of late-stage radiogenic Os is difficult to constrain, evidence for open-system behavior during formation of the gabbro layer involving injection of new magma, particularly magma carrying a significant IPGE component, seems a distinct possibility.

In a detailed study of magnetic properties, Larson (1994) found that the basal part of the spinifex layer and the upper portions of the gabbro layer share a unique paleopole different in orientation from any other part of the BCF. This paleopole is not explicable as a magnetic reversal, but could imply a change in direction of magma flow during the crystallization of Fe–Ti oxides in these rocks. Changes in spinifex orientation from perpendicular to subparallel to the layering were noted previously.

The aggregate weight of compositional reversals, simultaneous and localized enrichment in both IPGE and PPGE, open-system behavior in Re–Os systematics, and the sharing of a unique paleopole by lower spinifex and upper gabbro are considered highly suggestive of late-stage recharge in the magmatic evolution of the BCF.

## Conclusions

The main conclusions of this study are summarized as follows:

1. The spinifex clinopyroxene is very Ca-rich augite. It shows small core-to-rim variations over the middle part (13–20 m depth) and larger variations over the basal third of the spinifex interval, where Fe, Cr and Mn increase in rims. This effect is attributed to reaction between primary magmatic pyroxene and trapped intercumulus melt.

2. Two generations of clinopyroxene, primary spinifex augite and secondary embayment diopside and hedenbergite and overgrowth Ca- and Fe-rich augite, are present.

3. Mirror image profiles of Si and Al shown by core domains of spinifex clinopyroxene suggest substitution of Al for Si. Mutual exchange of ferrous Fe and Mg in specific sites of the pyroxene structure is also suggested by complementary profiles of these elements.

4. Comparison of clinopyroxene and whole-rock profiles show little indication that changes in melt composition are reflected in clinopyroxene composition, although exceptions occur in the case of Mn and perhaps Cr.

5. Whole-rock profiles indicate that elements compatible in clinopyroxene, such as Cr, Ni and Co, were efficiently removed from the magma in the upper 3 m of the spinifex layer, whereas highly incompatible elements are strongly partitioned into the melt.

6. In the basal 10 m of the spinifex layer, distinct compositional reversals characterize the behavior of Mg, Al and Cr. These may reflect recharge and mixing of unfractionated basaltic magma with fractionated residual melt.

7. An increase in whole-rock PGE–Cu–S contents at a depth of 20 m in the spinifex layer, along with aspects of Re–Os isotope systematics and magnetic character near the top of the gabbro layer, support the suggestion of injection of new magma during the formation of the gabbro layer.

## Acknowledgements

Dave Leng is grateful for the highly proficient assistance of Dr. Yves Thibault, formerly with the Department of Geology, University of Western Ontario, with the electron-microprobe analyses. The financial assistance of NSERC in the form of a Discovery Grant to JHC is greatly appreciated. WES is grateful for research support from the Australian Research Council in the form of a Discovery Project DP0345971 and for logistical support and encouragement from Geoinformatics Exploration Canada Limited. Finally, it is a pleasure to acknowledge the collaboration of Dr. Mike Fleet as a coauthor on six of our previous publications on the Boston Creek ferropicrite.

## References

Arndt, N.T. (1986): Differentiation of komatiite flows. *J. Petrol.* **27**, 279-301.

_____ & Fleet, M.E. (1979): Stable and metastable pyroxene crystallization in layered komatiite lava flows. *Am. Mineral.* **70**, 40-51.

_____ & Fowler, A.D. (2004): Textures in komatiites and variolitic basalts. *In* The Precambrian Earth: Tempos and Events (K. Eriksson, W. Altermann, D.R. Nelson, W.U. Mueller & O. Catuneanu, eds.). Elsevier, Amsterdam, The Netherlands (298-311).

Barnes, S.-J., Gorton, M.P. & Naldrett, A.J. (1983): A comparative study of olivine and clinopyroxene spinifex flows from Alexo, Abitibi greenstone belt, Ontario, Canada. *Contrib. Mineral. Petrol.* **83**, 293-308.

Brandeis, G. & Marsh, B.D. (1989): The convective liquids in a solidifying magma chamber: a fluid dynamic investigation. *Nature* **339**, 613-616.

Campbell, I. H. & Arndt, N. (1982): Pyroxene accumulation in spinifex-textured rocks. *Geol. Mag.* **119**, 605-610.

Corfu, F., Krogh, T.E., Kwok, Y.Y. & Jensen, L.S. (1989): U–Pb geochronology in the southwestern Abitibi greenstone belt, Superior Province. *Can. J. Earth Sci.* **26**, 1747-1763.

_____ & Noble, S.R. (1992): Genesis of the southern Abitibi greenstone belt, Superior Province, Canada: evidence from zircon Hf-isotope analyses using a single filament technique. *Geochim. Cosmochim. Acta* **56**, 2527-2531.

Crocket, J.H. (2002): Platinum-group element geochemistry of mafic and ultramafic rocks. *In* The Geology, Geochemistry, Mineralogy and Mineral Beneficiation of Platinum-Group Elements (L.J. Cabri, ed.). *Can. Inst. Mining Metall. Petroleum, Spec. Vol.* **54**, 177-210.

Donaldson, C.H. (1982): Spinifex-textured komatiites: a review of textures, compositions and layering. *In* Komatiites (N.T. Arndt & E.G. Nisbet, eds.). Allen & Unwin, London, U.K. (213-244).

Dostal, J., Dupuy, C., Carron, J.P., Le Guen de Kerneizon, M. & Maury, R.C. (1983): Partition coefficients of trace elements: application to volcanic rocks of St. Vincent, West Indies. *Geochim. Cosmochim. Acta* **47**, 525-533.

Fleet, M.E. (1974): Partition of major and minor elements in equilibration in coexisting pyroxenes. *Contrib. Mineral. Petrol.* **44**, 259-274.

Good, D.J., Crocket, J.H. & Barnett, R.L. (1997): A secondary clinopyroxene – chlorite – spinel assemblage in clinopyroxenite of the Mann Complex, Abitibi Belt, Ontario: an unusual hydrothermal alteration suite. *Mineral. Petrol.* **59**, 69-90.

Grove, T.L. & Bryan, W.B. (1983): Fractionation of pyroxene-phyric MORB at low pressure: an experimental study. *Contrib. Mineral. Petrol.* **84**, 293-309.

Hanski, E.J. (1992): Petrology of the Pechenga ferropicrites and cogenetic, Ni-bearing gabbro–wehrlite intrusions, Kola Peninsula, Russia. *Geol. Surv. Finland, Bull.* **367**.

Houle, M.G., Lesher, C.M. & Gibson, H.L. (2004): The significance of spinifex textures in constraining the mode of emplacement of Precambrian komatiitic and ferropicritic rocks: the Boston Creek sill. *Geol. Assoc. Can. – Mineral. Assoc. Can., Program Abstr.* **29**, 417.

JOLLY, W.T. (1980): Development and degradation of Archean lavas, Abitibi area, Canada, in light of major element geochemistry. *J. Petrol.* **21**, 323-363.

KEAYS, R.R. & LIGHTFOOT, P.C. (1999): The role of meteorite impact, source rocks, protores and mafic magmas in the genesis of the Sudbury Ni–Cu–PGE sulphide ore deposits (R.R. Keays, C.M. Lesher, P.C. Lightfoot & C.E.G. Farrow, eds.). *Geol. Assoc. Can., Short Course Vol.* **13**, 329-366.

KINZLER, R.J. & GROVE, T.L. (1985): Crystallization and differentiation of Archean komatiite lavas from northeast Ontario: phase equilibrium and kinetic studies. *Am. Mineral.* **70**, 40-51.

LARSON, M.S. (1994): *Geophysical Response of Sulfide-Poor PGM-Bearing Mafic-Ultramafic Rocks: Example of the Boston Creek Flow, Abitibi Greenstone Belt, Ontario*. B.Sc. thesis, McMaster Univ., Hamilton, Ontario.

_____, STONE, W.E., MORRIS, W.A. & CROCKET, J.H. (1998): Magnetic signature of magnetite-enriched rocks hosting platinum-group element mineralization within the Archean Boston Creek flow, Ontario. *Geophysics* **63**, 440-445.

LENG, D.M. (1997): *Mineralogical and Geochemical Study of an Unusual Clinopyroxene Spinifex Zone, Boston Creek Flow, Boston Township, Ontario*. B.A. thesis, McMaster Univ., Hamilton, Ontario.

LINDSLEY, D.H. & ANDERSEN, D.J. (1983): A two-pyroxene thermometer. *J. Geophys. Res.* **88**, A887-A906.

LINDSTROM, D.J. & WEILL, D.F. (1978): Partitioning of transition metals between diopside and coexisting silicate liquids. I. Nickel, cobalt, and manganese. *Geochim. Cosmochim. Acta* **42**, 817-831.

MANNING, C.E. & BIRD, D.K. (1986): Hydrothermal clinopyroxenes of the Skaergaard intrusion. *Contrib. Mineral. Petrol.* **92**, 437-447.

MARTIN, D., GRIFFITHS, R.W. & CAMPBELL, I.H. (1987): Compositional and thermal convection in magma chambers. *Contrib. Mineral. Petrol.* **96**, 465-475.

MCDONOUGH, W.F. & SUN, S.-S. (1995): The composition of the Earth. *Chem. Geol.* **120**, 223-253.

MORIMOTO, N. (1989): Nomenclature of pyroxenes. *Can. Mineral.* **27**, 143-156.

ROLLINSON, H.R. (1993): *Using Geochemical Data: Evaluation, Presentation, Interpretation*. Longman, London, U.K.

SHORE, M. & FOWLER, A.D. (1999): The origin of spinifex texture in komatiites. *Nature* **397**, 691-694.

STONE, W.E., CROCKET, J.H., DICKIN, A.P. & FLEET, M.E. (1995b): Origin of Archean ferropicrites: geochemical constraints from the Boston Creek flow, Abitibi greenstone belt, Ontario, Canada. *Chem. Geol.* **121**, 51-71.

_____, _____ & FLEET, M. (1993): Sulfide-poor platinum-group mineralization in komatiitic systems: Boston Creek flow, layered basaltic komatiite, Abitibi belt, Ontario. *Econ. Geol.* **88**, 817-836.

_____, _____ & _____ (1995a): Differentiation processes in an unusual iron-rich alumina-poor Archean ultramafic/mafic igneous body, Ontario. *Contrib. Mineral. Petrol.* **119**, 287-300.

_____, _____, _____ & LARSON, M.S. (1996): PGE mineralization in Archean volcanic systems: geochemical evidence from thick, differentiated mafic-ultramafic flows, Abitibi greenstone belt, Ontario, and implications for exploration. *J. Geochem. Explor.* **56**, 237-263.

_____, DELOULE, E., BERESFORD, S.W. & FIORENTINI, M. (2005): Anomalously high δD values in an Archean ferropicritic melt: implications for magma degassing, Abitibi Belt, Ontario: evidence for shallow degassing of Archean magma. *Can. Mineral.* **43**, 1745-1758.

_____, _____ & STONE, M. (2003): Hydromagmatic amphibole in komatiitic, tholeiitic and ferropicritic units, Abitibi greenstone belt, Ontario and Quebec: evidence for Archaean wet basic and ultrabasic melts. *Mineral. Petrol.* **77**, 39-65.

_____, FLEET, M.E., CROCKET, J.H. & KINGSTON, D.M. (1992): Platinum-group minerals in pyroxenite from the Boston Creek Flow basaltic komatiite, Abitibi greenstone belt, Ontario. *Can. Mineral.* **30**, 109-120.

_____, JENSEN, L.S. & CHURCH, W.R. (1987): Petrography and geochemistry of an unusual Fe-rich basaltic komatiite from Boston Township, northeastern Ontario. *Can. J. Earth Sci.* **24**, 2537-2550.

WALKER, R.J. & STONE, W.E. (2001): Os isotopic constraints on the origin of the 2.7 Ga Boston Creek flow, Ontario, Canada. *Chem. Geol.* **175**, 567-579.

*Received August 10, 2004, revised manuscript accepted October 1, 2005.*